



Research papers

Intra-oceanic island arc origin for Iratsu eclogites of the Sanbagawa belt, central Shikoku, southwest Japan

Atsushi Utsunomiya ^{a,*}, Bor-ming Jahn ^a, Kazuaki Okamoto ^b, Tsutomu Ota ^c, Hironao Shinjoe ^d^a Institute of Earth Sciences, Academia Sinica, Academia Road 2-128, Nankang, Taipei 11529, Taiwan^b Faculty of Education, Saitama University, Saitama 338-8570, Japan^c Institute for Study of the Earth's Interior, Okayama University, Misasa, Tottori 682-0193, Japan^d Faculty of Business Administration, Tokyo Keizai University, Tokyo 185-8502, Japan

ARTICLE INFO

Article history:

Received 19 May 2010

Received in revised form 1 November 2010

Accepted 2 November 2010

Available online 7 November 2010

Edited by R.L. Rudnick

Keywords:

Eclogites

Sanbagawa belt

Isotopic geochemistry

Oceanic island arc

ABSTRACT

New geochemical and Sr–Nd isotopic data for the Iratsu eclogite and surrounding metamorphic rocks of the Sanbagawa belt, Japan, show that, while the protoliths of the metamorphic rocks formed in a variety of tectonic settings, the Iratsu body represents a deeply subducted and accreted island arc. The igneous protoliths of eclogites and garnet amphibolites were probably generated from a mantle source that had components of both a depleted mantle modified by slab-released fluid (as seen in a negative Nb anomaly) and an enriched mantle, similar to that of ocean island basalts (OIB). Fractional crystallization modeling indicates that the protoliths of some garnet clinopyroxenites from the Iratsu body are cumulates from a basaltic magma that crystallized under high O₂ and H₂O fugacities in the middle to lower crust. The source characteristics and crystallization conditions suggest that the protoliths of the Iratsu rocks formed in an oceanic island arc. Quartz eclogites from the marginal zone of the Iratsu body have geochemical signatures similar to turbidites from the Izu–Bonin island arc (as seen in a negative Nb anomaly and a concave REE pattern). The protoliths might be volcaniclastic turbidites that formed in a setting proximal to the oceanic island arc. Geochemical and isotopic signatures of the surrounding mafic schists are similar to normal (N-) and enriched (E-) mid-ocean-ridge basalt (MORB), and distinct from the rocks from the Iratsu body. The protoliths of the mafic schists likely formed in a plume-influenced mid-ocean ridge or back-arc basin. Pelitic schists from the surrounding rocks and pelitic gneisses from the marginal zone of the Iratsu body have evolved, continental geochemical signatures (as seen in a negative $\varepsilon_{\text{Nd}}(t)$ value (~−5)), consistent with their origin as continent-derived trench-fill turbidites.

© 2010 Elsevier B.V. All rights reserved.

1. Introduction

Eclogites commonly occur in regional metamorphic belts of the Pacific-type (accretionary) orogens as a result of subduction of oceanic plate. Even though eclogites are volumetrically minor in any metamorphic belt, they are the principal rock type that bears evidence of high-pressure (HP) metamorphism. Eclogites are an important key to decipher the process and fate of oceanic plate subduction and to delineate the orogenic style along a plate convergent boundary.

The Sanbagawa belt of southwest Japan is a Cretaceous regional metamorphic belt. The belt is one of the best-documented Pacific-type metamorphic belts in the world (e.g., Banno and Sakai, 1989; Takasu et al., 1994; Aoya et al., 2003; Wallis et al., 2009). The belt has several eclogite-bearing bodies surrounded by non-eclogitic schists. These bodies had been recognized as tectonic blocks with

different origins from the surrounding schists, and the eclogite-facies metamorphism was considered unrelated to the Sanbagawa regional metamorphism (e.g., Takasu et al., 1994). However, recent field and petrological studies led to a different idea that the Sanbagawa eclogites were part of the accretionary complex, just the same as surrounding schists. They were then together subjected to the Sanbagawa metamorphism (Wallis and Aoya, 2000; Ota et al., 2004; Terabayashi et al., 2005). Despite numerous studies on the metamorphic and deformation process, the origin and tectonic setting of the protoliths of the eclogite and associated rocks have not been fully understood (Aoya et al., 2006; Nozaki et al., 2006; Okamoto et al., 2000; Terabayashi et al., 2005). The issue is important for understanding not only the local tectonic evolution but also what happens in a deep part of subduction zone. In this paper, we employ the geochemical and Sr–Nd isotopic tracer techniques to unravel the origin and tectonic setting of the eclogites and related rocks from the Iratsu body and surrounding schists of the Sanbagawa metamorphic belt. We show that an island arc can be subducted to the depth comparable to the eclogite-facies P–T condition.

* Corresponding author. Tel.: +886 2 2783 9910; fax: +886 2 2783 9871.

E-mail address: uchii@earth.sinica.edu.tw (A. Utsunomiya).

2. Geological background

2.1. The Sanbagawa belt

The Sanbagawa belt extends over 800 km along southwest Japan (Fig. 1a). To the north, the Sanbagawa belt is separated from the Ryoke belt by the Median Tectonic Line, which is a major strike-slip fault dividing southwest Japan into the Inner and Outer zones (Fig. 1b and c; Isozaki and Maruyama, 1991). The Ryoke belt is a Cretaceous high-temperature and low-pressure (HT-LP) regional metamorphic belt. To the south, the Sanbagawa belt is bounded in part by a Jurassic accretionary complex (the Chichibu belt) and in part by a Cretaceous accretionary complex (the Shimanto belt). Sasaki and Isozaki (1992) discovered a thrust boundary between the Sanbagawa belt and the

underlying Shimanto belt. Kawato et al. (1991) found a normal fault boundary of the Sanbagawa belt between the Sanbagawa belt and overlying Chichibu belt. The Sanbagawa metamorphism is characterized by the high-pressure and low-temperature (HP-LT) intermediate type (e.g., Banno and Sakai, 1989; Enami et al., 1994). The belt is generally non-eclogitic, but eclogite-facies metamorphism has been identified in two areas in the Shikoku island: the Besshi and Kotsu areas (red stars in Fig. 1b).

2.2. The Sanbagawa schists

The Sanbagawa belt consists mainly of meta-sedimentary rocks and mafic schists. Most meta-sedimentary rocks are pelitic to psammitic schists and phyllites, with rare metacherts (quartz schists)

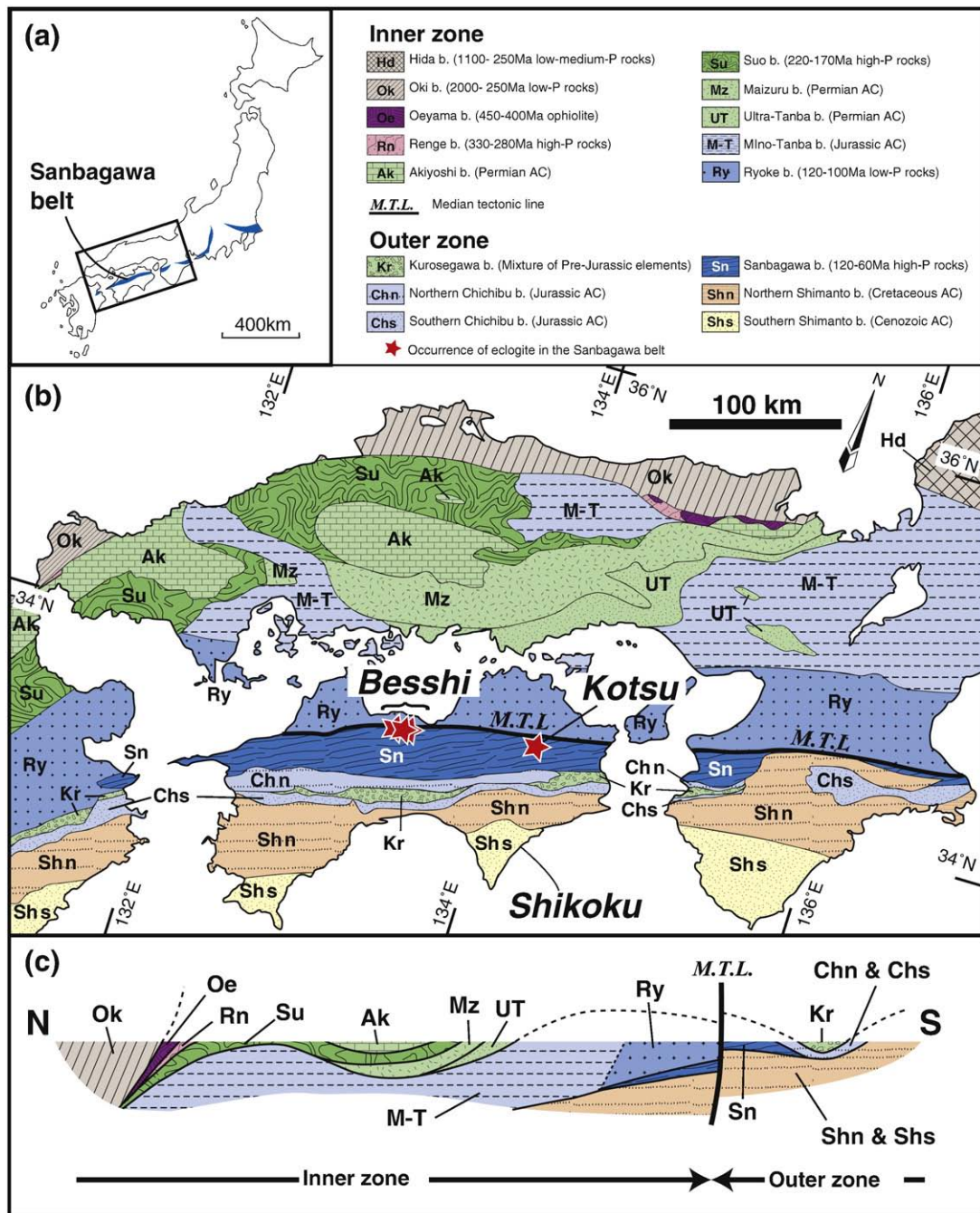


Fig. 1. Geological outline of the Sanbagawa belt (after Isozaki, 1996); (a) distribution of the Sanbagawa belt, (b) geotectonic subdivision of southwest Japan, and (c) schematic geotectonic profile of southwest Japan. AC = accretionary complex.

and calcareous schists. The mafic schists have basaltic compositions. The Sanbagawa schists in the Besshi area show a duplex structure formed during subduction (Okamoto et al., 2000). The lithologic characters and stratigraphy correspond to the upper part of oceanic plate (Okamoto et al., 2000). The geochemical characteristics of the meta-basaltic rocks from the Besshi area show the affinity of mid-ocean-ridge basalt (MORB; Nozaki et al., 2006; Okamoto et al., 2000). Overall, the protoliths of the Sanbagawa schists are an accreted part of oceanic plate.

Published K-Ar and Ar-Ar dates of hornblende and phengite, and fission track ages of zircons indicate that the Sanbagawa schists underwent cooling process from 95 to 65 Ma (Itaya and Takasugi, 1988; Takasu and Dallmeyer, 1990; Wallis, et al., 2004). The peak stage of the Sanbagawa metamorphism was considered to be at

116 ± 10 Ma based on an Rb-Sr whole-rock isochron age for high-grade pelitic schists (Minamishin, 1979).

2.3. The eclogite-bearing bodies in the Sanbagawa belt

The highest-grade part of the Sanbagawa belt includes several eclogite-facies metagabbro (Iratsu, Seba and Tonaru) and peridotite (Higashi-Akaishi) bodies (Fig. 2a). These bodies had been regarded as exotic tectonic blocks derived from the lower crust-wedge mantle of the hanging-wall base on the following arguments: (1) the eclogitic rocks occurs as isolated bodies, (2) the belt as a whole is of a HP-LT intermediate type metamorphism, even the highest grade (epidote-amphibolite facies) did not achieve the eclogite-facies condition, and

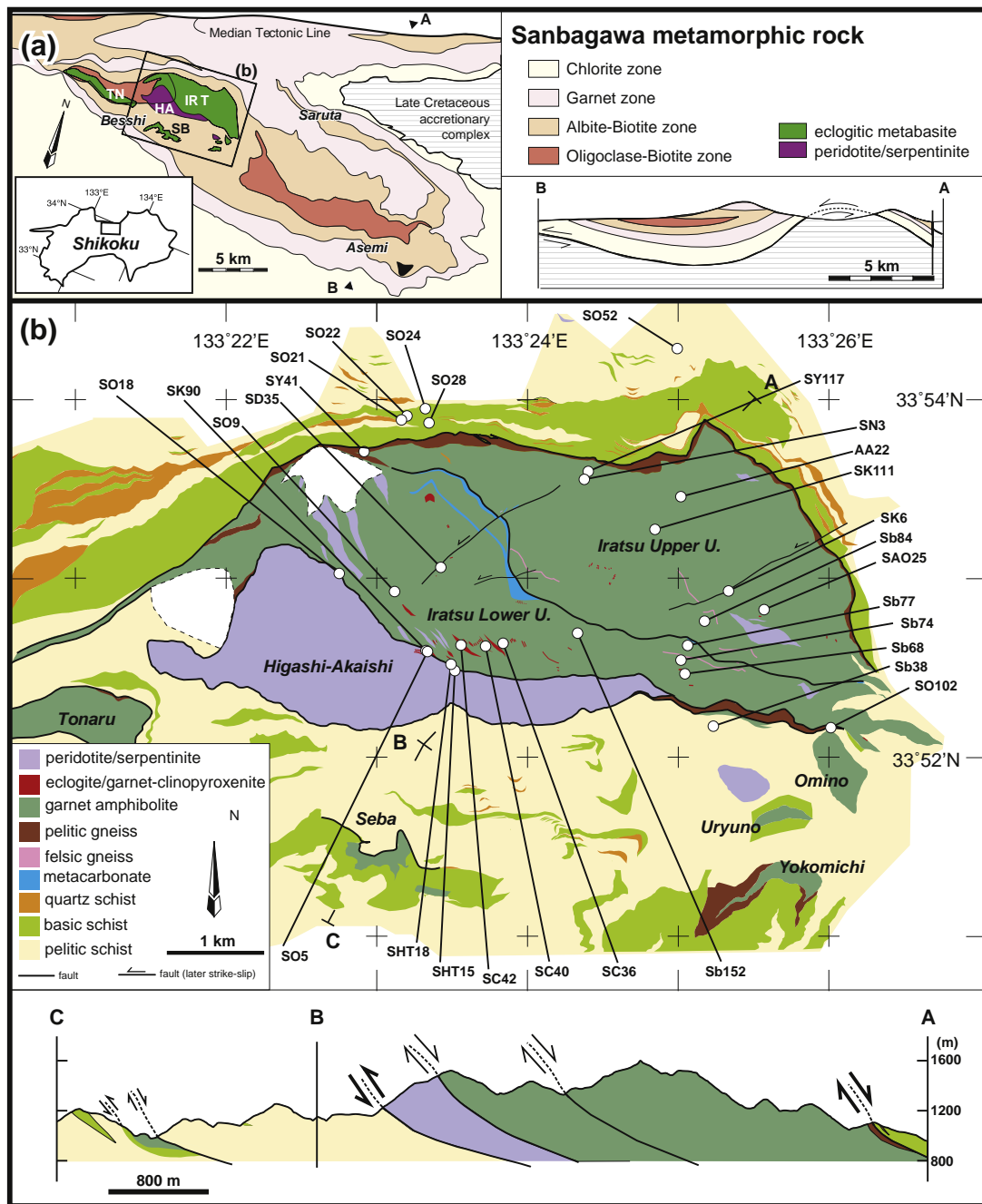


Fig. 2. (a) Metamorphic zones and profile of the Sanbagawa belt in central Shikoku (after Higashino, 1990). HA = Higashi-Akaishi body; IRT = Iratsu body; SB = Seba body; TN = Tonaru body. (b) Lithological map and profile around the Iratsu body in the Besshi area (after Ota et al., 2004; Yamamoto et al., 2004). Omino, Uryuno and Yokomichi metagabbro bodies do not bear eclogites and garnet clinopyroxenites due to a strong amphibolitization.

(3) the eclogitic bodies have a complicated thermal history including granulite-facies metamorphism (e.g., Takasu et al., 1994).

On the other hand, eclogitic schists were newly found in the surrounding schist in the Seba and Kotsu areas (Wallis and Aoya, 2000). The discovery implies that the eclogite-facies metamorphism is more widespread than previously thought. The Iratsu eclogitic and Higashi-Akaishi ultramafic bodies have a thermobaric structure concordant with the surrounding schists (Ota et al., 2004) and show a duplex structure formed during subduction-accretion (Terabayashi et al., 2005). Furthermore, the eclogite-facies metamorphism was thought to result from the geotherm of the surface of subducted slab (Aoya et al., 2003; Ota et al., 2004). The protoliths of the eclogites, ultramafic rocks and surrounding schists are considered to be accreted materials derived from oceanic domain (Terabayashi et al., 2005). It has been argued that the protoliths of these eclogites and ultramafic rocks were of an oceanic plateau origin in view of the presence of garnet-granulite relics and the close association with limestones (Terabayashi et al., 2005). On the other hand, using major and some trace element data, Aoya et al. (2006) proposed an oceanic island origin for the Seba metagabbro. However, some important data, such as rare earth element (REE) abundances and Nb and Sr-Nd isotopic ratios, were not obtained and considered.

The available Ar-Ar and K-Ar ages for minerals of the eclogite and eclogitic metagabbro from the Seba body are similar to those of the surrounding non-eclogitic schist (e.g., Dallmeyer and Takasu, 1991). The time of peak metamorphism is still an open question. Metamorphic zircons in quartz-bearing rocks from the marginal zone of the Iratsu body were dated at 110–130 Ma and the age range was regarded as the time of peak metamorphism of eclogite (Okamoto et al., 2004). In contrast, Lu-Hf isochron ages of 89–88 Ma were obtained for the eclogitic schists from Kotsu and Seba and the ages were regarded as the time of peak metamorphism (Wallis et al., 2009). However, another Lu-Hf isochron age of ~116 Ma was reported soon afterwards for the eclogites from the Iratsu body and the age was regarded as pre-peak metamorphism (epidote amphibolite-facies; Endo et al., 2009). The Nikubuchi cumulus ultramafic complex in the Iratsu body was dated at 138 ± 18 Ma by the Sm-Nd whole-rock isochron method and the age was regarded as the time of igneous event or the granulite-facies metamorphism before the Sanbagawa metamorphism (Senda et al., 2006).

2.4. Mode of occurrence of the Iratsu body

The Iratsu body in the Besshi area is the largest eclogite-bearing body. The Iratsu body is composed of eclogites and garnet clinopyroxenites and small amount of ultramafic rocks, rare meta-carbonates, felsic gneisses and quartz schists. Most eclogites and garnet clinopyroxenites are retrograded into garnet amphibolites. A map-scale distribution shows that the occurrence of eclogites and garnet clinopyroxenites is concentrated near the Higashi-Akaishi ultramafic body in the lower unit (Fig. 2b). In the Iratsu body, the eclogites and garnet clinopyroxenites occur as blocks of variable sizes, ranging from hand-specimen to meter-size scale (Ota et al., 2004). In the northern and southeastern margin, the Iratsu body is fringed by pelitic gneisses. Between the Iratsu and Higashi-Akaishi bodies, quartz eclogites occur as lenses. Meta-carbonates occur at the top of lower unit along the boundary of the upper unit.

3. Sample description

We conducted geochemical and isotopic analyses on the following rock types: eclogites (Fig. 3a), garnet clinopyroxenites and garnet amphibolites (= retrograded eclogites and garnet clinopyroxenite; Fig. 3b); all from the Iratsu body. In addition, quartz eclogites and pelitic gneisses (Fig. 3c and d) from the marginal zone of the Iratsu

body, and surrounding mafic (Fig. 3e) and pelitic schists (Fig. 3f) were also analyzed.

Ota et al. (2004) carried out a petrological study on eclogites and garnet clinopyroxenites. Eclogite generally shows fine- to medium-grained granoblastic textures. The mineral assemblage of peak metamorphism is garnet + omphacite + epidote + quartz + rutile ± calcic-sodic amphibole. Phenite and paragonite are observed in some eclogites. Calcic-sodic amphibole and ilmenite occur as retrograde minerals in many samples. Garnet clinopyroxenite exhibits coarse-grained equigranular texture that might be inherited from gabbroic protoliths. The rocks are mainly composed of garnet and sodic augite with rare rutile. Epidote, calcic-amphibole and ilmenite occur as retrograde minerals. Some eclogites and garnet clinopyroxenites bear garnet-granulite relics characterized by the coarse-grained poikiloblastic garnet with diopside inclusions (Ota et al., 2004). In garnet amphibolite, clinopyroxene was totally replaced by calcic-amphibole or symplectite of calcic-amphibole + quartz or + plagioclase.

Quartz eclogite is composed of poikiloblastic quartz with inclusions of garnet, omphacite, kyanite, phengite, epidote, and rutile. The paragenesis of pelitic gneisses includes large mica flakes, porphyroblasts of plagioclase and garnet and some quartz and titanite.

Mafic schist has a metamorphic mineral assemblage of amphibole + plagioclase + epidote + phengite + titanite + quartz. The rock does not preserve igneous relics. Pelitic schist is composed of garnet + quartz + plagioclase + phengite + biotite.

4. Analytical procedure

Samples were crushed in a stainless steel mill and then powdered in an agate mill. The powdered samples were mixed with lithium tetraborate ($\text{Li}_2\text{B}_4\text{O}_7$) flux that was ten times as much as the sample, fused in a platinum crucible and cast into a glass bead. Major element compositions were determined by X-ray fluorescence (XRF) techniques on fused glass beads, using a Rigaku RIX2000 spectrometer at the Department of Geosciences, National Taiwan University. A detailed XRF analytical procedure was described by Lee et al. (1997). The analytical quality is shown in Appendix A.

For trace elements analyses, we used the same fused powdered samples into for XRF analysis. Pieces of fused glass beads were dissolved using a HF-HNO₃ (2:1) mixture in a screw-top Teflon beaker for >2 h at ~100 °C, followed by evaporation to dryness, and then dissolved using 1:2 HNO₃ for a night at ~100 °C. This procedure was followed by evaporation to dryness and re-dissolved in 2% HNO₃ before inductively coupled plasma-mass spectrometer (ICP-MS) analysis. Trace elements were measured using an ICP-MS (Agilent 7500s) at the Department of Geosciences, National Taiwan University. A more detailed ICP-MS analytical procedure can be found in Yang et al. (2005). The duplicate analyses on five rock standards AGV-1, AGV-2, GSP-1, JB-1 and JG-1 showed that the accuracy was better than 10% for most elements (Yang et al., 2005). The within-run precision was generally better than 5% (2σ) for most elements.

For Sr-Nd isotopic analysis, powdered samples were dissolved using a HF-HNO₃ (2:1) mixture in a screw-top Teflon beaker for 2 days at ~100 °C. This procedure was followed by evaporation to dryness, refluxing in 6 N HCl and drying twice, and then dissolution in 1 N HCl. The procedure was repeated until complete dissolution. Chemical separation was carried out using the conventional ion exchange techniques. Sr and Nd isotope ratios were measured using a Finnigan MAT 262 and a TRITON mass spectrometer at the Institute of Earth Sciences, Academia Sinica. The effect of mass fractionation in Sr and Nd isotopic measurements was corrected by normalizing to $^{86}\text{Sr}/^{88}\text{Sr} = 0.1194$ and $^{146}\text{Nd}/^{144}\text{Nd} = 0.7219$. Analyses of NBS 987 Sr and JMC Nd standard throughout the period of analysis yielded $^{86}\text{Sr}/^{87}\text{Sr} = 0.710238 \pm 0.000016$ (2σ) and $^{143}\text{Nd}/^{144}\text{Nd} = 0.511812 \pm 0.000007$ (2σ). Procedural blanks were approximately 330 pg Sr and

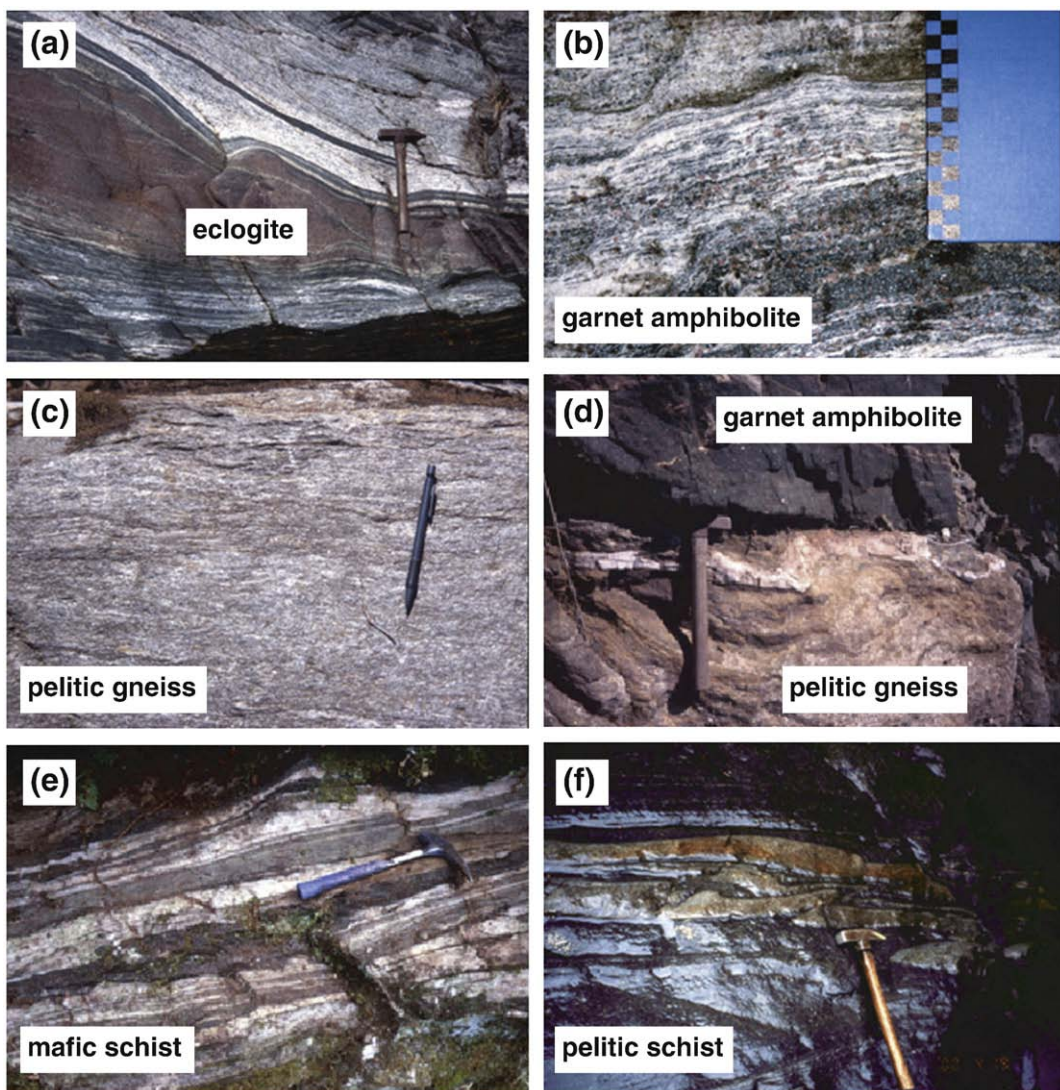


Fig. 3. Photographs showing field occurrence of the metamorphic rocks from the Besshi area; (a) eclogite from the Iratsu body occurs as layers in gneissose amphibolites, (b) garnet amphibolite from the Iratsu body encloses porphyroblastic garnet, (c) pelitic gneiss from the marginal zone of the Iratsu body shows coarse-grained mica flake, (d) sharp contact between garnet amphibolite and pelitic gneiss, (e) mafic schists from the surrounding Sanbagawa schists, and (f) pelitic schists from the surrounding schists.

300 pg Nd. Within-run precision, expressed as $2\sigma_m$ was better than 0.000010 for both Sr and Nd.

5. Results

5.1. Eclogites, garnet clinopyroxenites and garnet amphibolites from the Iratsu body

Geochemical analyses for the rocks from the Besshi area are shown in Table 1. Fig. 4 is selected major element oxides vs. SiO₂ variation diagrams. Eclogites have higher SiO₂ contents (45–49%) than garnet clinopyroxenites (40–43%). SiO₂ contents of garnet amphibolites overlap with the ranges of both eclogites and garnet clinopyroxenites (41–50%). Eclogites, garnet clinopyroxenites and garnet amphibolites plot on broad linear trend on MgO and Fe₂O₃* vs. SiO₂ diagrams. MgO and Fe₂O₃* generally decrease with increasing SiO₂. TiO₂ shows a small range of variation ($\sim 1 \pm 0.4\%$). Al₂O₃ of eclogites and garnet clinopyroxenites seems to decrease with increasing SiO₂. However, Al₂O₃ contents of most garnet amphibolites are higher than those of eclogites and garnet clinopyroxenites. CaO contents of garnet clinopyroxenites are constant, whereas those of eclogites and garnet amphibolites are scattered.

Fig. 5 shows REE patterns of rocks from the Iratsu body. Eclogites and garnet amphibolites have similar REE patterns (Fig. 5a and b). They show two kinds of light (L) REE distribution; enriched and flat. However, all heavy (H) REE patterns are nearly flat and parallel. In Fig. 5c, some garnet clinopyroxenites have REE patterns similar to eclogites, but others have lower REE abundance and show more pronounced depletion in LREE and marked positive Eu anomalies.

Fig. 6 shows the spidergrams for refractory trace elements of rocks from the Iratsu body. Spidergrams of eclogites and garnet amphibolites that have flat REE patterns show negative Nb and Zr-Hf anomalies (Fig. 6a and b). The samples that have LREE-enriched REE patterns (SD35, SK111, SK6 and SO9) show less negative Nb anomalies and little to no negative Zr-Hf anomalies. Although some garnet clinopyroxenites have spidergram patterns similar to eclogites, others are distinguished from the eclogites. They show much lower abundance and highly fractionated patterns characterized by negative Nb anomalies, distinct negative Zr-Hf anomalies, and positive Ti anomalies (Fig. 6c).

The Sr-Nd isotopic data for the rocks from the Besshi area are given in Table 2. $\varepsilon_{\text{Nd}}(t)$ and I_{Sr} values are calculated at 120 Ma based on the SHRIMP U-Pb zircon metamorphic age for the Iratsu body (Okamoto et al., 2004). Eclogites, garnet clinopyroxenites and garnet

Table 1

Major and trace element compositions of eclogites and related rocks from the Besshi area.

Sample	AA22	SAO25	Sb68	Sb74	Sb77	Sb84	Sb152	SC36	SC40	SC42	SD35	SK6	SK90	SK111
Complex	The Iratsu body													
LAT. (°N) ^a	33.8930	33.8827	33.8768	33.3780	33.8793	33.8817	33.8806	33.8794	33.8792	33.8794	33.8866	33.8844	33.8788	33.8897
LNG. (°E) ^a	133.4144	133.4233	133.4148	133.4144	133.4151	133.4171	133.4029	133.3947	133.3928	133.3902	133.3875	133.4196	133.3863	133.4114
Lithology	EC	GAM	EC	GCP	GCP	GAM	EC	GCP	GCP	GCP	EC	GAM	GCP	EC
T (°C) ^b	607		660	664	683		659	673	743	664	650			591
(wt.%)														
SiO ₂	45.35	43.24	44.51	42.93	42.24	42.94	46.54	41.41	40.59	40.84	48.84	49.66	39.92	46.85
TiO ₂	1.31	1.37	1.01	1.05	1.34	0.87	0.65	0.86	0.84	0.91	0.96	1.03	1.20	1.35
Al ₂ O ₃	16.48	13.90	17.01	16.24	16.01	24.54	15.89	17.45	19.00	17.93	14.75	19.31	19.13	16.39
Fe ₂ O ₃ *	18.21	20.00	14.06	16.20	18.90	11.68	11.44	15.69	15.99	17.65	8.77	10.80	19.53	13.49
MnO	0.29	0.22	0.28	0.19	0.18	0.26	0.17	0.21	0.30	0.28	0.20	0.20	0.33	0.23
MgO	5.78	9.12	7.64	7.77	7.14	4.85	6.21	9.40	8.27	8.04	4.01	4.76	7.09	4.60
CaO	10.39	11.54	12.20	14.00	13.31	12.51	14.71	14.11	14.22	14.33	17.08	8.81	14.26	12.37
Na ₂ O	2.71	0.78	2.37	1.05	0.75	2.20	3.38	0.81	0.88	0.30	1.75	3.46	0.11	3.45
K ₂ O	0.03	0.01	0.06	I.d.	0.04	0.11	0.05	0.01	0.05	I.d.	I.d.	0.47	I.d.	0.50
P ₂ O ₅	0.07	0.04	0.15	0.05	0.16	0.30	0.11	0.09	0.16	0.06	0.51	0.31	0.18	0.52
LOI	0.30	0.44	1.08	0.36	0.50	1.97	0.65	0.46	0.46	0.32	1.79	1.43	0.28	0.57
Total	100.92	100.65	100.38	99.84	100.57	102.23	99.79	100.47	100.75	100.67	98.64	100.26	102.04	100.30
(ppm)														
Sc	46.2	37.2	42.6	45.6	46.2	16.5	29.3	43.0	39.6	48.9	26.7	22.0	55.1	27.7
V	575	558	396	589	930	173	308	535	483	527	137	191	558	245
Cr	12.6	8.2	54.4	56.9	62.1	13.0	102.8	18.4	51.3	47.4	39.2	15.0	2.4	15.1
Co	33.9	87.3	40.5	54.7	60.5	22.8	33.1	54.3	48.7	45.3	24.3	29.8	46.3	30.5
Ni	12.2	76.1	32.0	27.6	32.3	9.6	34.5	19.4	32.3	20.1	24.0	15.2	10.8	11.8
Cu	40.2	195.2	20.5	41.9	110.0	29.3	67.1	17.2	38.9	52.6	113.7	28.2	26.9	13.2
Zn	110	113	110	87	106	59	84	74	110	80	107	118	98	103
Ga	19.8	13.2	17.5	18.2	19.3	22.1	19.3	15.8	18.1	13.5	15.3	22.1	13.3	17.7
Rb	0.52	0.37	0.46	0.28	0.41	1.26	0.32	0.55	0.20	0.35	0.52	2.64	0.28	5.03
Sr	385	123	427	371	325	816	651	68	259	61	618	702	44	462
Y	12.0	9.9	25.7	9.3	14.4	10.3	12.5	4.0	20.3	4.9	32.0	21.3	7.5	23.0
Zr	11.6	12.2	22.0	18.7	21.1	14.5	17.3	0.7	11.1	0.9	63.1	76.4	0.9	37.4
Nb	0.31	0.24	1.16	0.53	1.40	0.47	0.27	0.005	0.54	0.07	13.03	4.54	0.17	3.02
Cs	0.24	0.11	0.38	0.21	0.13	0.57	0.14	0.14	0.06	0.25	0.29	0.54	0.19	0.40
Ba	29.0	6.6	27.0	16.8	7.0	91.9	7.5	20.6	10.0	2.8	5.9	259.6	1.3	163.1
La	2.79	1.09	3.90	1.82	6.18	2.26	1.74	0.26	6.52	0.44	18.63	14.57	0.55	12.65
Ce	6.69	3.65	12.99	4.97	15.59	5.70	5.29	0.35	15.39	1.23	49.54	31.81	1.78	30.00
Pr	1.07	0.72	2.30	0.83	2.18	1.00	1.01	0.10	2.21	0.23	7.10	4.39	0.36	4.32
Nd	5.46	4.19	12.08	4.26	9.55	5.75	5.58	0.64	10.68	1.42	31.37	19.79	2.31	19.99
Sm	1.74	1.46	3.56	1.38	2.44	1.80	1.85	0.34	3.03	0.58	7.25	4.78	0.91	4.76
Eu	0.76	0.47	1.17	0.56	0.65	1.00	0.62	0.24	0.99	0.36	1.61	1.53	0.51	1.37

Gd	1.84	1.45	3.66	1.51	2.41	1.85	1.91	0.56	3.10	0.68	6.97	4.57	1.09	4.57	
Tb	0.32	0.27	0.63	0.26	0.40	0.29	0.32	0.11	0.51	0.13	1.01	0.67	0.21	0.65	
Dy	2.20	1.81	4.39	1.73	2.51	1.90	2.02	0.72	3.45	0.96	5.95	3.89	1.36	3.84	
Ho	0.47	0.41	0.96	0.36	0.54	0.40	0.43	0.16	0.77	0.21	1.20	0.78	0.31	0.81	
Er	1.27	1.08	2.66	0.98	1.48	1.07	1.16	0.39	2.17	0.56	3.15	2.11	0.82	2.29	
Tm	0.19	0.16	0.41	0.14	0.22	0.16	0.18	0.06	0.33	0.09	0.42	0.30	0.12	0.33	
Yb	1.22	0.98	2.68	0.89	1.42	0.98	1.13	0.33	2.23	0.57	2.66	1.96	0.75	2.19	
Lu	0.18	0.14	0.39	0.13	0.20	0.15	0.17	0.05	0.35	0.09	0.38	0.29	0.12	0.32	
Hf	0.42	0.47	0.91	0.54	0.77	0.45	0.62	0.05	0.45	0.05	2.00	1.93	0.05	1.07	
Ta	0.023	0.011	0.040	0.041	0.128	0.027	0.015	0.123	0.046	0.019	1.076	0.263	0.018	0.230	
W	0.15	1.71	0.16	0.17	0.29	0.90	0.27	0.19	0.14	0.24	0.54	0.22	0.27	0.15	
Pb	1.18	1.01	1.92	0.87	2.69	1.17	2.20	0.27	1.61	0.54	3.69	6.72	1.03	4.34	
Th	0.074	0.014	0.021	0.030	0.141	0.005	0.030	0.003	0.133	0.035	3.926	0.091	0.000	0.867	
U	0.020	0.005	0.005	0.013	0.048	0.004	0.016	0.004	0.035	0.039	1.062	0.088	0.019	0.388	
Sample	SN3	S05	S09	SO18	SY117	SHT15	SHT18	SO102	SY41	SO21	SO22	SO24	SO28	Sb38	SO52
Complex	The Iratsu body					Marginal zone of the Iratsu body				Surrounding schist					
LAT. (°N) ^a	33.8946	33.8788	33.8845	33.8860	33.8953	33.8770	33.8777	33.8717	33.8970	33.9001	33.9003	33.9010	33.8999	33.8720	33.9070
LNG. (°E) ^a	133.4038	133.3865	133.3831	133.3769	133.4041	133.3895	133.3890	133.4305	133.3794	133.3836	133.3843	133.3865	133.3869	133.4179	133.4136
Lithology	EC	GAM	GAM	GCP	GAM	QEC	QEC	PG	PG	MS	MS	MS	MS	PS	PS
T (°C) ^b	650			695											
(wt.%)															
SiO ₂	44.87	41.35	49.73	41.37	44.79	64.42	51.89	64.88	64.35	48.36	46.66	43.26	46.78	64.31	67.71
TiO ₂	1.42	1.06	1.47	1.37	0.80	0.50	0.52	0.71	0.70	1.88	1.19	1.00	2.32	0.63	0.59
Al ₂ O ₃	18.18	21.49	18.14	16.93	19.89	13.88	13.66	14.99	17.15	16.36	17.67	12.48	14.98	16.14	15.61
Fe ₂ O ₃ *	16.56	13.05	10.22	17.79	13.04	8.34	10.82	6.24	6.38	11.36	11.99	10.81	13.14	5.40	5.45
MnO	0.22	0.16	0.30	0.26	0.22	0.14	0.20	0.13	0.13	0.15	0.18	0.19	0.18	0.11	0.18
MgO	5.84	5.02	5.95	8.23	6.30	3.54	10.12	2.78	1.94	5.26	4.10	11.08	8.13	1.95	1.85
CaO	11.08	12.77	6.40	14.34	12.50	4.96	8.81	2.69	0.80	11.28	12.26	11.64	8.82	2.65	0.37
Na ₂ O	2.04	2.49	3.45	0.54	2.14	1.76	2.26	2.28	1.40	2.54	2.85	2.79	1.76	2.41	2.00
K ₂ O	0.03	0.14	2.16	l.d.	0.10	1.03	0.68	2.43	3.35	0.56	1.01	0.15	0.59	2.78	3.38
P ₂ O ₅	0.32	0.61	0.43	0.04	0.05	0.10	0.09	0.16	0.09	0.21	0.15	0.10	0.23	0.15	0.11
LOI	0.49	1.49	1.37	0.24	1.05	0.66	0.44	3.17	3.59	1.14	1.23	7.06	2.69	3.50	2.81
Total	101.04	99.63	99.63	101.11	100.88	99.34	99.48	100.44	99.86	99.10	99.28	100.56	99.63	100.02	100.05
(ppm)															
Sc	36.9	24.3	29.0	47.2	44.7	38.1	42.0	28.4	30.9	31.6	38.1	26.1	39.4	29.1	33.1
V	416	237	135	676	322	141	253	77	85	237	234	145	282	83	70
Cr	5.1	15.7	112.5	23.7	16.1	48.3	388.6	102.7	59.4	83.4	484.7	616.6	67.4	49.2	41.5
Co	37.1	27.5	29.5	45.2	38.9	17.4	39.5	13.8	11.5	41.3	47.4	54.4	43.5	10.8	11.9
Ni	9.8	16.0	114.3	12.7	15.1	20.8	100.0	67.4	26.4	50.8	203.1	379.7	40.4	22.7	26.9
Cu	60.8	42.2	27.8	80.8	76.0	27.0	29.3	21.9	32.2	74.7	25.4	13.4	69.9	36.4	40.7
Zn	109	112	105	98	92	86	80	70	113	92	372	83	91	73	78
Ga	20.7	21.8	20.1	17.4	19.8	12.7	13.5	17.5	20.7	19.2	15.9	13.2	19.4	18.3	19.0
Rb	0.55	1.42	66.41	0.37	0.74	13.27	9.65	97.40	133.6	9.86	17.49	2.68	17.12	107.2	143.3

(continued on next page)

Table 1 (continued)

Sample	SN3	SO5	SO9	SO18	SY117	SHT15	SHT18	SO102	SY41	SO21	SO22	SO24	SO28	Sb38	SO52
Complex															
The Iratusu body															
LAT. (°N) ^a	33.8946	33.8788	33.8845	33.8860	33.8953	33.8770	33.8777	33.8717	33.8970	33.9001	33.9003	33.9010	33.8999	33.8720	33.9070
LNG. (°E) ^a	133.4038	133.3865	133.3831	133.3769	133.4041	133.3895	133.3890	133.4305	133.3794	133.3836	133.3843	133.3865	133.3869	133.4179	133.4136
Lithology	EC	GAM	GAM	GCP	GAM	QEC	QEC	PG	PG	MS	MS	MS	MS	PS	PS
T (°C) ^b	650			695											
(ppm)															
Sr	388	821	279	51	523	154	88	167	166	351	220	78	254	177	54
Y	23.7	15.7	35.4	5.0	22.3	24.6	16.6	29.5	42.4	24.8	28.4	17.4	33.4	24.9	22.9
Zr	30.2	9.9	191.6	1.5	16.8	65.6	31.0	163.6	157.0	119.6	78.7	53.6	153.7	159.4	145.2
Nb	1.20	0.76	29.96	0.13	0.81	1.62	0.80	12.70	11.12	11.69	2.97	2.55	12.88	11.66	11.05
Cs	2.36	0.31	1.90	0.13	0.41	0.25	0.52	4.49	7.44	0.30	0.60	0.20	4.88	4.80	9.42
Ba	19.1	55.6	493.9	4.1	33.6	163.9	41.1	409.2	604.3	30.4	42.8	14.0	55.1	428.8	478.0
La	5.02	3.69	33.69	0.67	2.65	8.63	3.39	28.36	53.89	9.30	3.93	2.67	10.65	28.62	16.49
Ce	13.36	10.19	64.90	1.74	8.00	17.81	7.61	58.95	62.58	22.08	9.59	7.04	26.36	59.74	58.83
Pr	2.17	1.77	7.82	0.29	1.51	2.34	1.08	6.77	10.98	3.11	1.70	1.15	3.88	6.64	4.17
Nd	11.09	9.72	29.98	1.66	8.59	10.16	5.11	25.08	40.52	14.26	8.73	5.91	17.92	24.26	15.58
Sm	3.29	2.87	6.41	0.54	2.82	2.71	1.61	5.20	7.57	3.91	2.88	1.98	4.91	4.73	3.40
Eu	1.05	1.06	1.86	0.33	0.98	0.83	0.56	1.16	1.84	1.33	1.07	0.64	1.67	1.12	0.77
Gd	3.62	2.85	6.80	0.68	2.99	3.05	1.92	5.34	8.09	4.23	3.46	2.33	5.34	4.92	3.72
Tb	0.60	0.46	0.98	0.13	0.54	0.52	0.35	0.78	1.09	0.69	0.64	0.44	0.89	0.68	0.57
Dy	3.98	2.77	5.77	0.85	3.56	3.61	2.51	4.73	6.25	4.25	4.38	2.84	5.62	4.18	3.50
Ho	0.86	0.58	1.24	0.19	0.79	0.87	0.58	0.99	1.32	0.88	0.99	0.59	1.22	0.88	0.77
Er	2.29	1.51	3.42	0.50	2.24	2.55	1.73	2.78	3.74	2.33	2.76	1.60	3.23	2.50	2.22
Tm	0.35	0.20	0.51	0.07	0.34	0.40	0.26	0.42	0.54	0.33	0.42	0.24	0.48	0.40	0.35
Yb	2.16	1.24	3.43	0.47	2.22	2.78	1.76	2.78	3.43	2.15	2.72	1.56	3.14	2.65	2.28
Lu	0.32	0.18	0.53	0.07	0.32	0.44	0.28	0.42	0.50	0.30	0.40	0.23	0.46	0.39	0.35
Hf	0.99	0.38	4.46	0.07	0.71	1.76	0.89	4.14	4.01	2.68	1.85	1.32	3.52	4.14	3.75
Ta	0.067	0.029	2.059	0.002	0.086	0.078	0.041	1.031	0.897	0.833	0.228	0.186	0.917	0.949	0.930
W	0.21	0.15	0.56	0.24	0.16	0.14	0.05	0.69	0.60	0.17	0.40	0.02	0.32	0.56	1.13
Pb	1.10	3.82	17.20	0.17	2.99	1.67	1.18	14.35	17.44	1.14	1.24	0.13	0.90	15.37	22.35
Th	0.035	0.040	8.823	0.025	0.006	1.676	0.649	11.53	11.27	0.845	0.227	0.189	0.983	12.03	12.09
U	0.016	0.019	2.083	0.009	0.004	0.506	0.092	2.32	2.20	0.285	0.249	0.095	0.292	2.54	2.40

Fe_2O_3^* = total Fe as Fe_2O_3 ; LOI = loss on ignition.

l.d. = lower than detection limit.

EC = eclogite; GCP = garnet clinopyroxenite; GAM = garnet amphibolite; QEC = quartz eclogite; PG = pelitic gneiss; MS = mafic schist; PS = pelitic schist.

^a Estimated by using a sample locality map made on a scale of 1 to 5000 with coordinate information provided by Google Map (<http://maps.google.co.jp/>).

^b Metamorphic temperature at a given pressure of 20 kbar estimated by Ota et al. (2004).

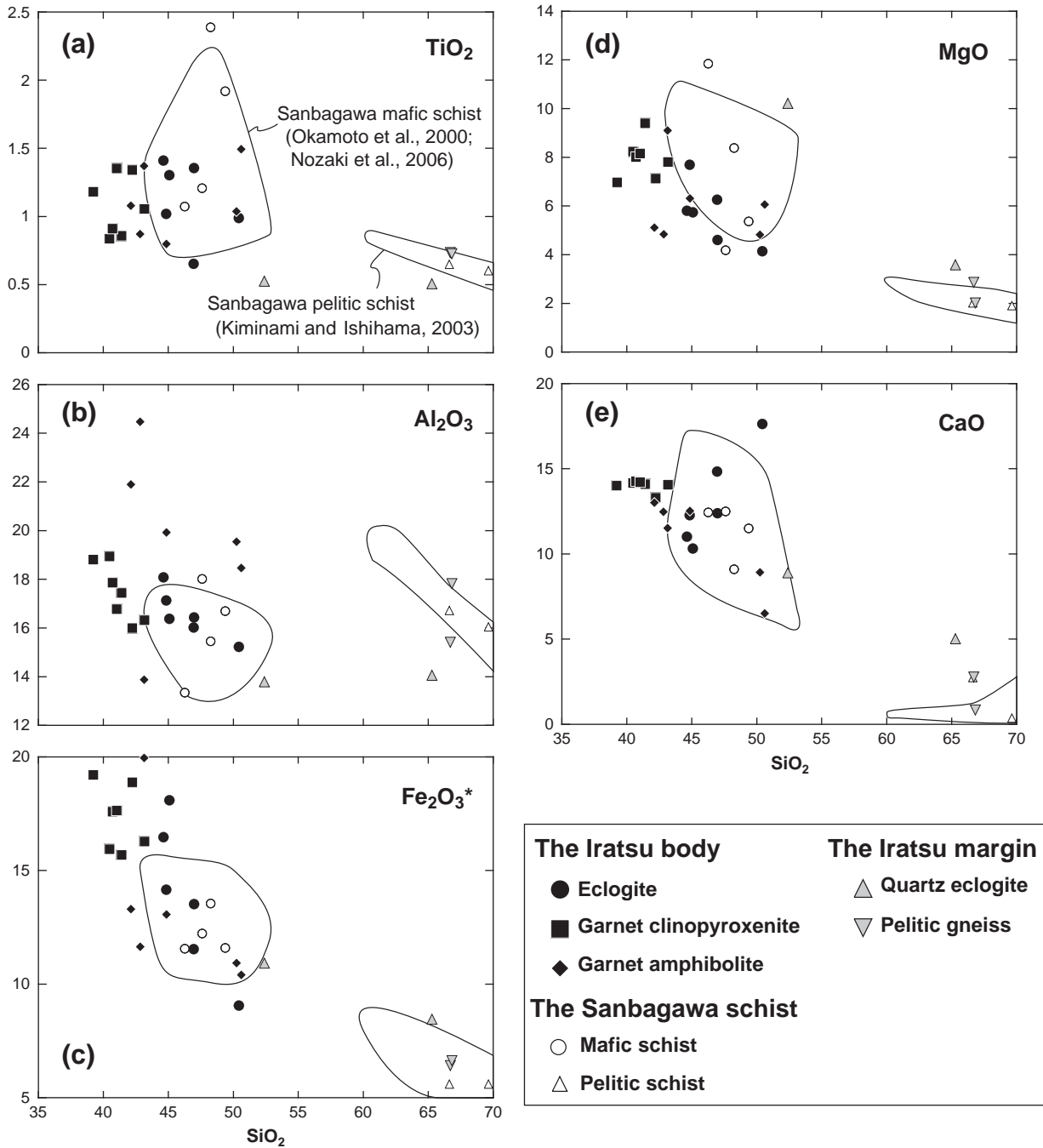


Fig. 4. Major element oxides vs. SiO_2 variation diagrams for rocks from the Besshi area. The values are reported on the anhydrous basis, recalculated to 100%. Also shown are the fields of the Sanbagawa pelitic schists from the Asemi area (dataset from Kiminami and Ishihama, 2003) and the Sanbagawa mafic schists from the Besshi area (dataset from Okamoto et al., 2000; Nozaki et al., 2006).

amphibolites show a negative correlation on $\varepsilon_{\text{Nd}}(\text{t})$ and I_{Sr} diagram (Fig. 7). The Sr-Nd isotopic data fall in the fields of oceanic island basalts (OIB) and continental arc. Many of them also plot in the field of "oceanic island arc basalt".

5.2. Rocks from the margin of the Iratsu body and surrounding Sanbagawa Schists

In Fig. 4, pelitic schists of the Sanbagawa belt from the Besshi area plot in the field defined for the schists from Asemi area, east-central Shikoku (Kiminami and Ishihama, 2003). Pelitic gneisses from the marginal zone of the Iratsu body are chemically comparable to the

pelitic schists from the surrounding Sanbagawa schists. In terms of trace elements distribution, the pelitic gneisses are similar to the pelitic schists (Fig. 8). The REE patterns are LREE-enriched, flat HREE and show slightly negative Eu anomalies (Fig. 8a). The spidergram patterns exhibit negative Nb and Ti anomalies (Fig. 8b). Pelitic schists and pelitic gneisses show negative $\varepsilon_{\text{Nd}}(\text{t})$ values (-5.6 to -4.4 ; Fig. 7).

Two quartz eclogites show distinct SiO_2 contents, one at 65% and the other 53% (Fig. 4). The difference is due to the mode percentage of quartz. The high- SiO_2 sample (SHT15) has major element compositions similar to pelitic schists and pelitic gneisses. However, the REE pattern is distinguished from those of pelitic schists and pelitic

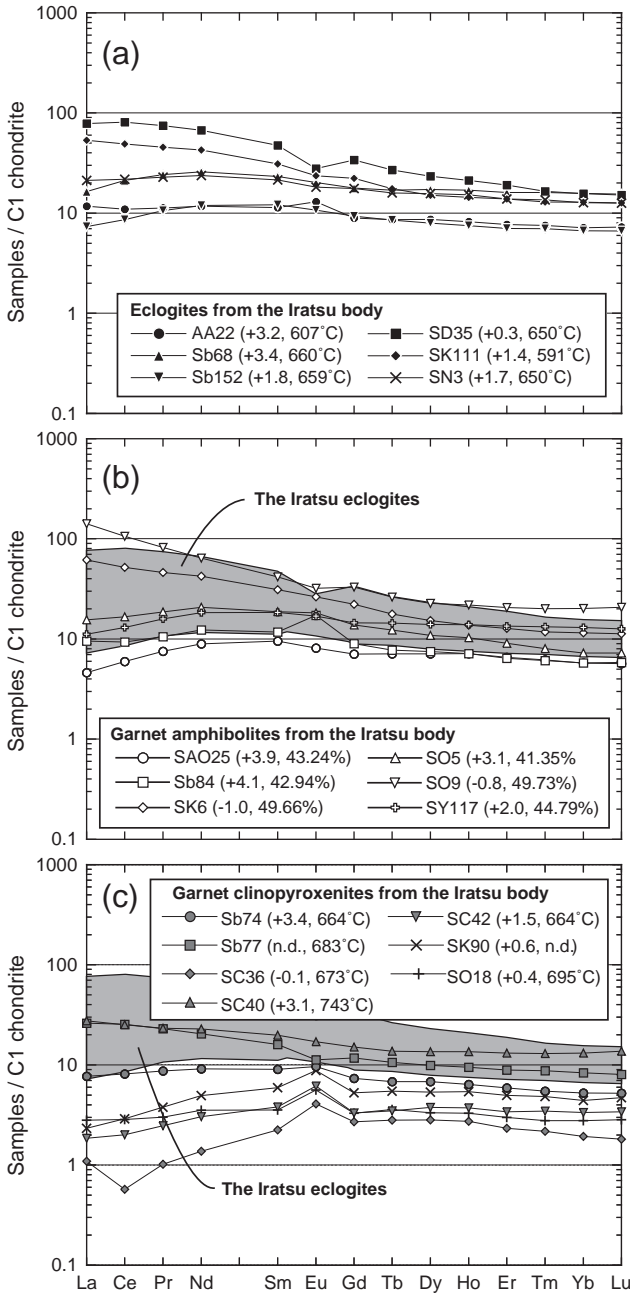


Fig. 5. REE patterns for rocks from the Iratsu body; (a) eclogites, (b) garnet amphibolites, and (c) garnet clinopyroxenites. The grey field in (b) and (c) indicates the fields of the Iratsu eclogites from (a). The parenthetic number with sample number of (a) and (c) indicates $\epsilon_{\text{Nd}}(t)$ value and metamorphic temperature estimated by Ota et al. (2004). The parenthetic number with sample number of (b) indicates $\epsilon_{\text{Nd}}(t)$ value and SiO₂ content. C1 chondrite values are from Sun and McDonough (1989).

gneisses. The high-SiO₂ sample shows slightly concave REE pattern (Fig. 8a). The spidergram pattern has remarkable negative Nb anomaly but weak negative Ti anomaly (Fig. 8b). The low-SiO₂ quartz eclogite (SHT18) corresponds to evolved (high-SiO₂) eclogites and garnet amphibolites. However, the low-SiO₂ quartz eclogite has a MgO higher than that of eclogites and garnet amphibolites. The REE and spidergram patterns of the low-SiO₂ quartz eclogite are distinguished from those of eclogites but similar to those of the high-SiO₂ quartz eclogite (Fig. 8a and b). Despite the big difference in major element compositions, quartz eclogites have an identical Nd isotopic composition ($\epsilon_{\text{Nd}}(t) = +6.4$; Fig. 7).

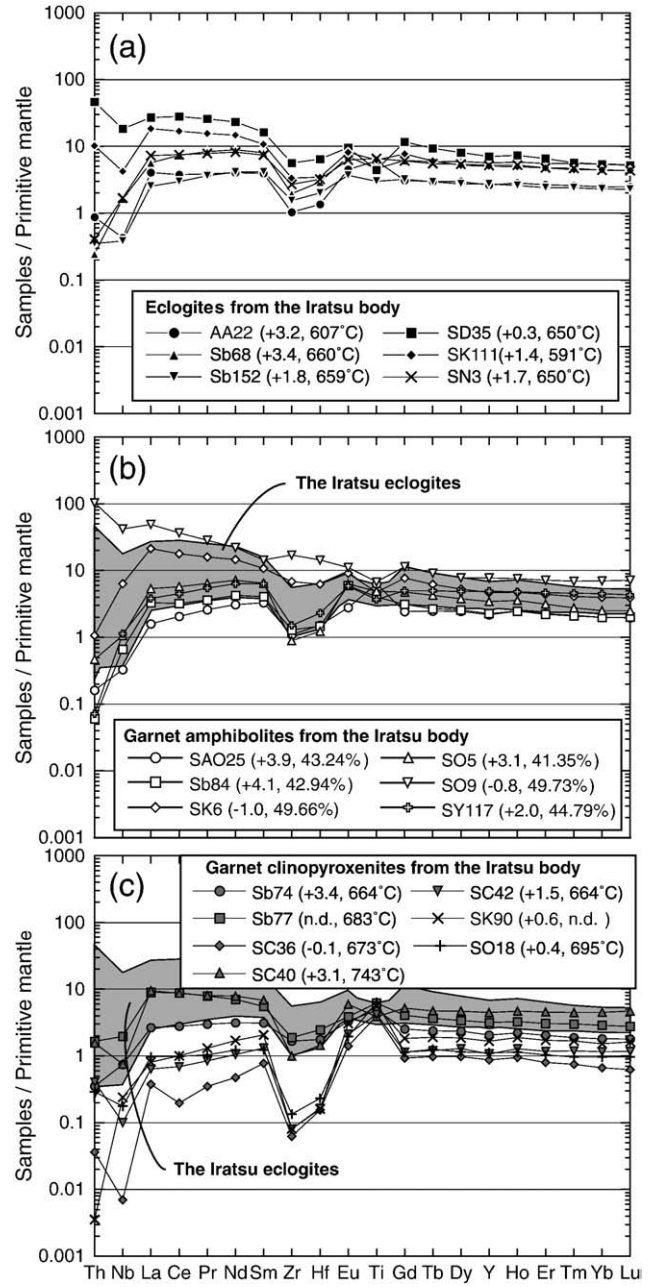


Fig. 6. Spidergrams for rocks from the Iratsu body; (a) eclogites, (b) garnet amphibolites, and (c) garnet clinopyroxenites. The grey field in (b) and (c) indicates the fields of the Iratsu eclogites from (a). The parenthetic number with sample number of (a) and (c) indicates $\epsilon_{\text{Nd}}(t)$ value and metamorphic temperature estimated by Ota et al. (2004). The parenthetic number with sample number of (b) indicates $\epsilon_{\text{Nd}}(t)$ value and SiO₂ content. Primitive mantle values are from Sun and McDonough (1989).

Mafic schists from the Besshi area are divided into high- and low-TiO₂ samples (Fig. 4). Low-TiO₂ samples have flat REE patterns, whereas high-TiO₂ ones have slightly LREE-enriched and flat HREE patterns (Fig. 9a). In spidergrams, mafic schists have smooth patterns and do not show any anomalies (Fig. 9b). The geochemical signatures of the mafic schists in this study are not distinguishable from those reported by previous studies (Okamoto et al., 2000; Nozaki et al., 2006). In terms of Sr-Nd isotopic compositions, mafic schists show a more depleted character ($\epsilon_{\text{Nd}}(t) = +5.3$ to $+6.8$; $I_{\text{Sr}} = 0.703$ – 0.705) than the rocks from the Iratsu body (Fig. 7). High-TiO₂ samples have slightly lower $\epsilon_{\text{Nd}}(t)$ than low-TiO₂ ones.

Table 2

Sr and Nd isotopic compositions of eclogite and related rocks from the Besshi area.

Sample no.	Area	Lithology	Rb	Sr	$^{87}\text{Rb}/^{86}\text{Sr}$	$^{87}\text{Sr}/^{86}\text{Sr}$	$2\sigma_m$	$\text{lsr}(120)$	Sm	Nd	$^{147}\text{Sm}/^{144}\text{Nd}$	$^{143}\text{Nd}/^{144}\text{Nd}$	$2\sigma_m$	$\varepsilon_{\text{Nd}}(0)$	$\varepsilon_{\text{Nd}}(120)$
AA22	Iratsu body	Eclogite	0.52	385	0.0039	0.704411	8	0.704411	1.74	5.46	0.1926	0.512797	7	+3.1	+3.2
SAO25	Iratsu body	Gt amphibolite	0.37	123	0.0088	0.704674	10	0.704674	1.46	4.19	0.2110	0.512849	11	+4.1	+3.9
Sb68	Iratsu body	Eclogite	0.46	427	0.0031	0.704446	8	0.704446	3.56	12.08	0.1779	0.512798	6	+3.1	+3.4
Sb74	Iratsu body	Gt clinopyroxenite	0.28	371	0.0021	0.704369	9	0.704369	1.38	4.26	0.1961	0.512814	6	+3.4	+3.4
Sb84	Iratsu body	Gt amphibolite	1.26	816	0.0045	0.704355	7	0.704355	1.80	5.75	0.1896	0.512842	6	+4.0	+4.1
Sb152	Iratsu body	Eclogite	0.32	651	0.0014	0.704801	9	0.704801	1.85	5.58	0.2005	0.512734	8	+1.9	+1.8
SC36	Iratsu body	Gt clinopyroxenite	0.55	68.2	0.0235	0.705479	9	0.705479	0.34	0.64	0.3243	0.512733	5	+1.9	-0.1
SC40	Iratsu body	Gt clinopyroxenite	0.20	259	0.0023	0.704186	9	0.704186	3.03	10.68	0.1717	0.512778	6	+2.7	+3.1
SC42	Iratsu body	Gt clinopyroxenite	0.35	60.6	0.0168	0.705544	9	0.705544	0.58	1.42	0.2487	0.512756	6	+2.3	+1.5
SD35	Iratsu body	Eclogite	0.52	618	0.0024	0.706173	8	0.706173	7.25	31.37	0.1398	0.512610	6	-0.5	+0.3
SK6	Iratsu body	Gt amphibolite	2.64	702	0.0109	0.706228	9	0.706228	4.78	19.79	0.1460	0.512548	7	-1.7	-1.0
SK90	Iratsu body	Gt clinopyroxenite	0.28	43.7	0.0185	0.705594	9	0.705594	0.91	2.31	0.2382	0.512701	7	+1.2	+0.6
SK111	Iratsu body	Eclogite	5.03	462	0.0315	0.704988	7	0.704987	4.76	19.99	0.1439	0.512668	6	+0.6	+1.4
SN3	Iratsu body	Eclogite	0.55	388	0.0041	0.704759	9	0.704759	3.29	11.09	0.1793	0.512711	7	+1.4	+1.7
S05	Iratsu body	Gt amphibolite	1.42	821	0.0050	0.704624	8	0.704624	2.87	9.72	0.1784	0.512781	6	+2.8	+3.1
S09	Iratsu body	Gt amphibolite	66.4	279	0.6897	0.707636	9	0.707624	6.41	29.98	0.1292	0.512546	7	-1.8	-0.8
S018	Iratsu body	Gt clinopyroxenite	0.37	50.9	0.0210	0.705375	10	0.705375	0.54	1.66	0.1988	0.512658	7	+0.4	+0.4
SY117	Iratsu body	Gt amphibolite	0.74	523	0.0041	0.704731	9	0.704731	2.82	8.59	0.1984	0.512741	6	+2.0	+2.0
SHT15	Iratsu margin	Qz Eclogite	13.3	154	0.2496	0.704261	7	0.704256	2.71	10.16	0.1614	0.512937	7	+5.8	+6.4
SHT18	Iratsu margin	Qz Eclogite	9.65	87.5	0.3191	0.705081	9	0.705075	1.61	5.11	0.1899	0.512960	6	+6.3	+6.4
SO102	Iratsu margin	Pelitic gneiss	97.4	167	1.6851	0.710793	7	0.710765	5.20	25.08	0.1253	0.512294	8	-6.7	-5.6
SY41	Iratsu margin	Pelitic gneiss	134	166	2.3268	0.711256	8	0.711216	7.57	40.52	0.1130	0.512347	6	-5.7	-4.4
SO21	Sanbagawa Schist	Mafic schist	9.86	351	0.0814	0.703310	8	0.703309	3.91	14.26	0.1658	0.512888	7	+4.9	+5.4
SO22	Sanbagawa Schist	Mafic schist	17.5	220	0.2295	0.704632	7	0.704628	2.88	8.73	0.1996	0.512950	7	+6.1	+6.0
SO24	Sanbagawa Schist	Mafic schist	2.68	77.7	0.0998	0.703955	7	0.703954	1.98	5.91	0.2022	0.512991	7	+6.9	+6.8
SO28	Sanbagawa Schist	Mafic schist	17.1	254	0.1953	0.703485	8	0.703482	4.91	17.92	0.1656	0.512885	6	+4.8	+5.3
Sb38	Sanbagawa Schist	Pelitic schist	107	177	1.7509	0.710120	8	0.710090	4.73	24.26	0.1178	0.512345	7	-5.7	-4.5
SO52	Sanbagawa Schist	Pelitic schist	143	54.3	7.6424	0.716063	8	0.715933	3.40	15.58	0.1319	0.512317	8	-6.3	-5.3

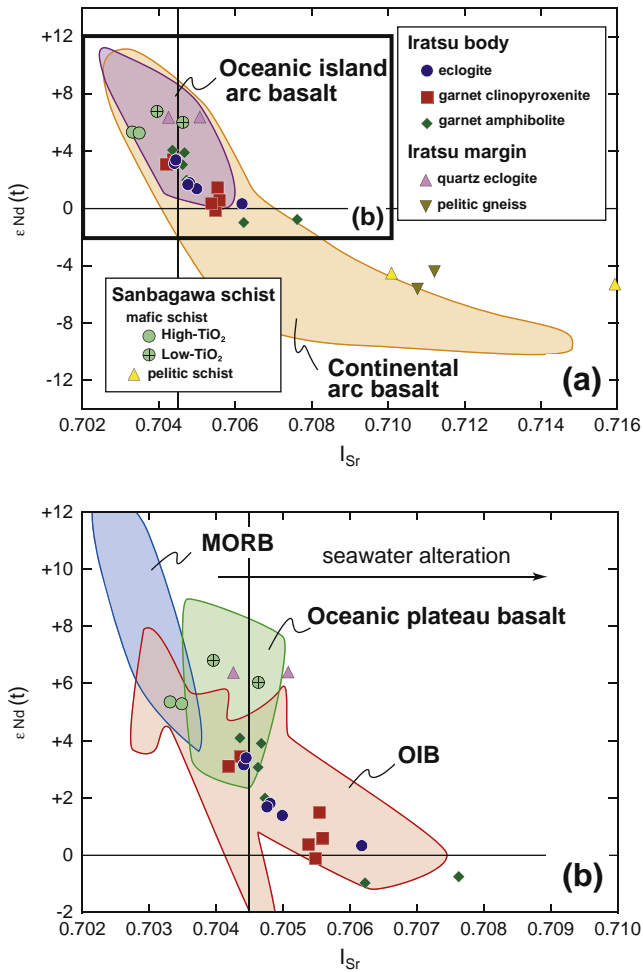


Fig. 7. $\epsilon_{\text{Nd}}(t)$ vs. I_{Sr} diagram for rocks from the Besshi area. $\epsilon_{\text{Nd}}(t)$ and $I_{\text{Sr}}(t)$ values are calculated at 120 Ma based on the SHRIMP U-Pb zircon metamorphic age for the Iratsu body (Okamoto et al., 2004). MORB, OIB and oceanic plateau basalts are from the compilation of Kogiso (2007). Oceanic and continental arc basalts are from the compilation of Kelemen et al. (2003).

6. Discussion and conclusions

6.1. Assessment of compositional modification by the pre-Sanbagawa and Sanbagawa metamorphism

The effect of seawater alteration prior to the Sanbagawa metamorphism may be discernible in an $\epsilon_{\text{Nd}}(t)$ vs. I_{Sr} diagram, because Sr isotopic composition is rather sensitive to seawater alteration, so the isotopic exchange with the seawater Sr would give rise to a shift of radiogenic Sr towards the seawater value (ca. 0.709) but little or no change in Nd isotopic composition (Jahn et al., 1980). Eclogites, garnet clinopyroxenites and garnet amphibolites show a good $\epsilon_{\text{Nd}}(t)$ - I_{Sr} correlation comparable to the oceanic basalt array, hence severe seawater alteration probably did not occur (Fig. 7).

During transition from blueschist to eclogite facies at about 1.5–2.5 GPa and 500–600 °C, no significant element transfer occurs, although the transition liberates a large amount of aqueous fluid (Spandler et al., 2003). The experimental study at 650–700 °C and 3 GPa showed that a significant amount of large ion lithophile elements (LILE) and Sr enter the aqueous fluid whereas REE, Th, U and high field strength elements (HFSE) are nearly retained (Green and Adam, 2003). On the other hand, the review of experimental and

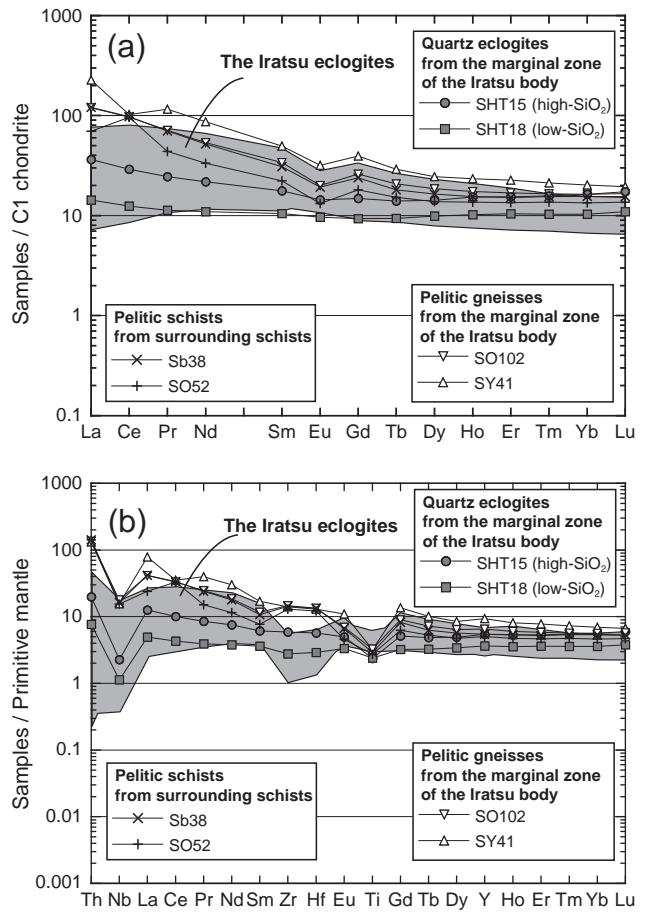


Fig. 8. (a) REE patterns and (b) spidergrams for quartz eclogites and pelitic gneisses from the marginal zone of the Iratsu body and pelitic schists from the surrounding Sanbagawa schists. The grey field indicates the Iratsu eclogites from Figs. 5a and 6a. C1 chondrite and primitive mantle values are from Sun and McDonough (1989).

petrological studies on the fluid phases in HP and ultrahigh pressure (UHP) metamorphic conditions by Hermann et al. (2006) showed that the critical temperature interval where the solubility of fluid phase strongly increases in subducted crust is at 700–750 °C at 100–150 km depth. Passing through the interval, release of fluid significantly modifies the chemical composition of host rock. Geothermobarometry for the peak metamorphism of most eclogites and garnet clinopyroxenites from the Iratsu body yielded conditions of 1.4–2.5 GPa and 500–700 °C. Some samples have recorded 700–800 °C at around 2.5 GPa (Ota et al., 2004) and this condition is near the critical temperature interval. However, the difference between LREE-enriched and flat REE patterns of the eclogites is not dependent on the metamorphic temperature (LREE-enriched = 590–650 °C; flat REE = 610–660 °C). Garnet clinopyroxenites having geochemical characteristics similar to the Iratsu eclogite share the metamorphic grade with highly fractionated ones (eclogite-like = 660–740 °C; highly fractionated = 660–700 °C). Therefore, the significant geochemical characteristics cannot be explained by compositional modification of HP prograde metamorphism.

REE patterns and spidergrams of garnet amphibolites are not more scattered than those of eclogites and garnet clinopyroxenites (Figs. 5 and 6). Besides, garnet amphibolites show a good $\epsilon_{\text{Nd}}(t)$ - I_{Sr} correlation with eclogites and garnet clinopyroxenites (Fig. 7). Consequently, the HFSE and REE abundances and Sr-Nd isotopic systems have not been significantly modified by the retrograde amphibolitization. The following discussion on tectonic significance will be based on the abundances and ratios of these elements and Sr-Nd isotope ratios.

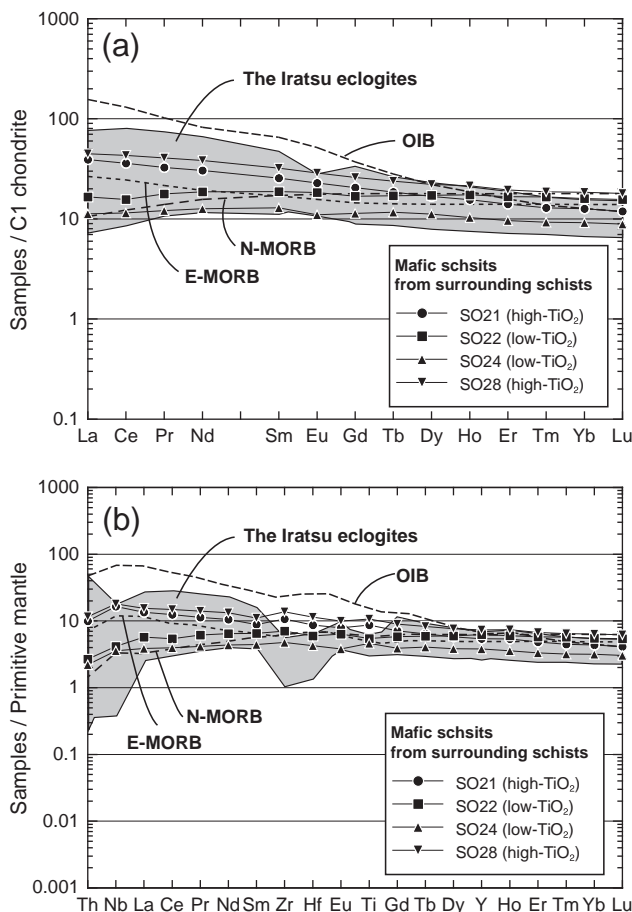


Fig. 9. (a) REE patterns and (b) spidergrams for mafic schists from the surrounding Sanbagawa schists. The grey field indicates the Iratsu eclogites from Figs. 5a and 6a. C1 chondrite and primitive mantle values and reference lines of N-MORB, E-MORB and OIB are from Sun and McDonough (1989).

6.2. Origin and tectonic setting of the protoliths of the Iratsu body

6.2.1. Origin of the protoliths of the Iratsu body

Because garnet clinopyroxenites have low SiO₂ contents (40–43%), they could not be melt but most likely of cumulate origin. On the other hand, eclogites have higher SiO₂ contents (45–49%), so they are probably of magma composition. Garnet amphibolites with high SiO₂ contents (>44%) might be retrograde eclogites, whereas those with low SiO₂ contents (<44%) are likely retrograde garnet clinopyroxenites.

The eclogites, garnet clinopyroxenites and garnet amphibolites from the Iratsu body do not have a uniform Nd isotopic composition ($\epsilon_{\text{Nd}}(t)$ = −1 to +4). This feature suggests that their protoliths were likely generated from mixed source, but in different proportion, between isotopically enriched (with relatively low $\epsilon_{\text{Nd}}(t)$ value) and depleted (with relatively high $\epsilon_{\text{Nd}}(t)$ value) sources. Eclogites and high-SiO₂ garnet amphibolites have two kinds of REE patterns; LREE-enriched and flat (Fig. 5a and b). LREE-enriched rocks have $\epsilon_{\text{Nd}}(t)$ = −1 to +1.5, whereas the rocks with flat REE patterns have $\epsilon_{\text{Nd}}(t)$ = +1.5 to +4 (Fig. 10a). The rocks with enriched Nd isotopic compositions (relative low $\epsilon_{\text{Nd}}(t)$) have also enriched REE characteristics. The rocks with higher $\epsilon_{\text{Nd}}(t)$ values and flat patterns have more depletion of HFSE than those with lower $\epsilon_{\text{Nd}}(t)$ values and LREE-enriched patterns (Fig. 10b and c). The LREE/HREE and HFSE/REE ratios of the eclogites and high-SiO₂ garnet amphibolites might represent the primary melt compositions, because the ratios correlate with $\epsilon_{\text{Nd}}(t)$ value, which is not changed during a fractional

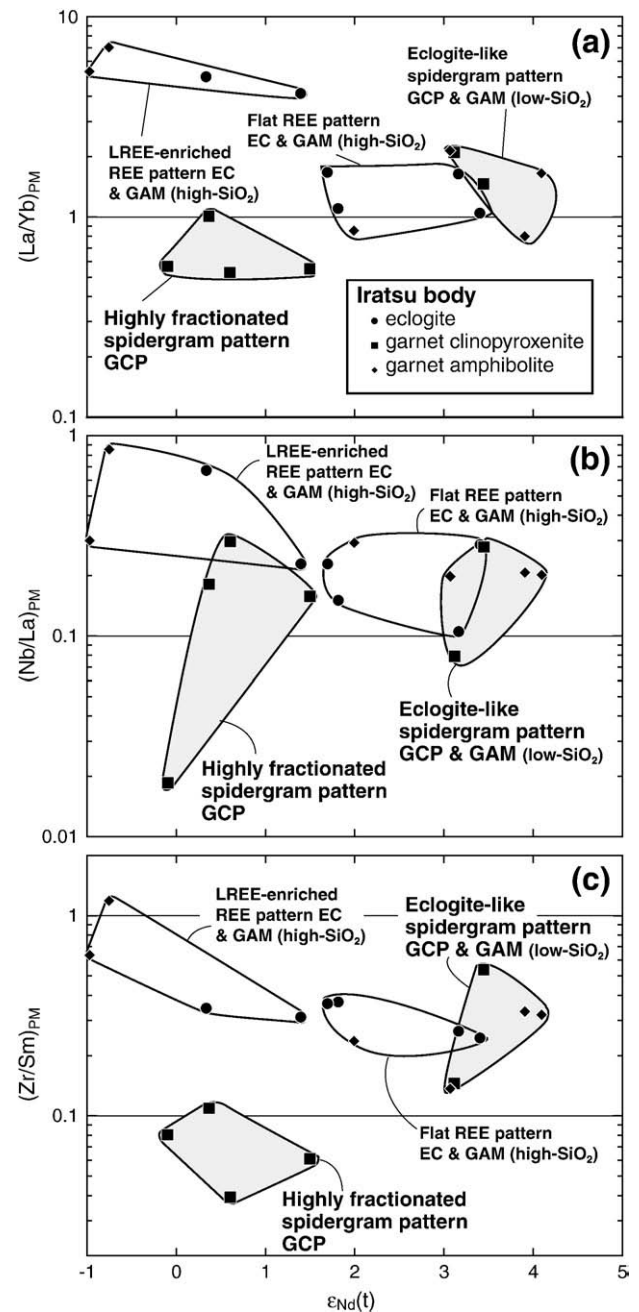


Fig. 10. Trace element ratios vs. $\epsilon_{\text{Nd}}(t)$ diagrams. GCP = garnet clinopyroxenite; GAM = garnet amphibolite. PM = ratio of values normalized to primitive mantle. The compositions of primitive mantle are from Sun and McDonough (1989).

crystallization. The correlations between $\epsilon_{\text{Nd}}(t)$ value and the LREE/HREE and HFSE/REE ratios argue that the protoliths of the rocks are generated by mixing of two components; a depleted component with HFSE depletion and an enriched component without HFSE depletion.

Table 3

Parameters used in the crystallization modeling.

Partition coefficient	La	Sm	Zr	Ti	Reference
Olivine	0	0.00044	0	0.01	Zanetti et al. (2004)
Orthopyroxene	0	0.022	0.02	0.12	Frei et al. (2009)
Clinopyroxene	0.051	0.33	0.16	0.36	Hauri et al. (1994)
Plagioclase ^a	0.21	0.12	0.002	0.058	Bindeman et al. (1998)
Magnetite	0	0.0072	0.046	14.5	Nielsen and Beard (2000)

^a Average of partition coefficient for plagioclases with high anorthite number (An#>70).

Table 4

Bulk partition coefficient and compositions of cumulate estimated by crystallization modeling.

Experimental condition	Solid fraction (%)	Mineral mode (%) (ol:opx:cpx:pl:mt)	Bulk partition coefficient				Cumulate composition (ppm)				
				La	Sm	Zr	Ti	La	Sm	Zr	Ti
Hamada and Fujii (2008)											
Anhydrous, 2 kbar	7	14:00:00:86:00	0.18	0.099	0.002	0.051	3.5	0.8	0.2	313	
Anhydrous, 2 kbar	32	31:00:00:69:00	0.14	0.079	0.003	0.043	3.7	0.8	0.3	356	
Anhydrous, 4 kbar	7	00:29:00:71:00	0.15	0.091	0.011	0.069	2.9	0.7	0.7	1.4	
Anhydrous, 4 kbar	25	00:36:00:64:00	0.13	0.082	0.010	0.062	3.2	0.8	0.8	1.5	
Anhydrous, 7 kbar	13	00:38:00:62:00	0.13	0.079	0.010	0.082	2.7	0.7	0.8	535	
Anhydrous, 7 kbar	55	00:25:24:49:02	0.11	0.14	0.047	0.41	4.1	1.9	6.2	3475	
2.7% H ₂ O, 2 kbar	3	33:00:00:00:67	0.002	0.005	0.032	9.7	0.0	0.0	2.1	44118	
2.7% H ₂ O, 2 kbar	20	30:00:00:55:15	0.11	0.064	0.009	2.2	2.6	0.6	0.7	10,231	
2.7% H ₂ O, 4 kbar	13	00:46:08:23:23	0.053	0.064	0.035	3.4	1.1	0.5	2.5	15,024	
2.7% H ₂ O, 4 kbar	31	00:26:23:39:13	0.092	0.13	0.050	2.0	2.4	1.3	4.5	8792	
2.7% H ₂ O, 7 kbar	8	00:63:25:00:13	0.014	0.097	0.062	2.0	0.3	0.8	4.2	10,544	
2.7% H ₂ O, 7 kbar	14	00:36:43:07:14	0.037	0.16	0.086	2.3	0.8	1.3	6.2	11,089	
2.7% H ₂ O, 7 kbar	41	00:20:27:41:12	0.10	0.14	0.055	1.9	3.0	1.6	5.7	8003	

ol = olivine; opx = orthopyroxene; cpx = clinopyroxene; pl = plagioclase; mt = magnetite.

6.2.2. Crystallization modeling for the cumulate rocks (garnet clinopyroxenites)

In Fig. 10, some garnet clinopyroxenites and low-SiO₂ garnet amphibolites plot on the mixing trend of eclogites and high-SiO₂ garnet amphibolites, other garnet clinopyroxenites with highly fractionated compositional characteristics are away from the mixing trend. To clarify which the highly fractionated garnet clinopyroxenites was formed from the mantle source same to those of eclogites and got away from the mixing trend by magmatic process or generated from

totally different source from other rocks, we test possible cumulate compositions by a modeling study with some assumptions and parameters given in Tables 3 and 4.

The degree of crystallization (solid fraction), mineral assemblage and mode percentage of the cumulate phase are referred to the melting experimental study on a basaltic starting material under anhydrous and hydrous and NNO-buffered fO₂ conditions at 2–7 kbar (Hamada and Fujii, 2008). The partition coefficient of olivine is from Zanetti et al. (2004), orthopyroxene from Frei et al. (2009) and

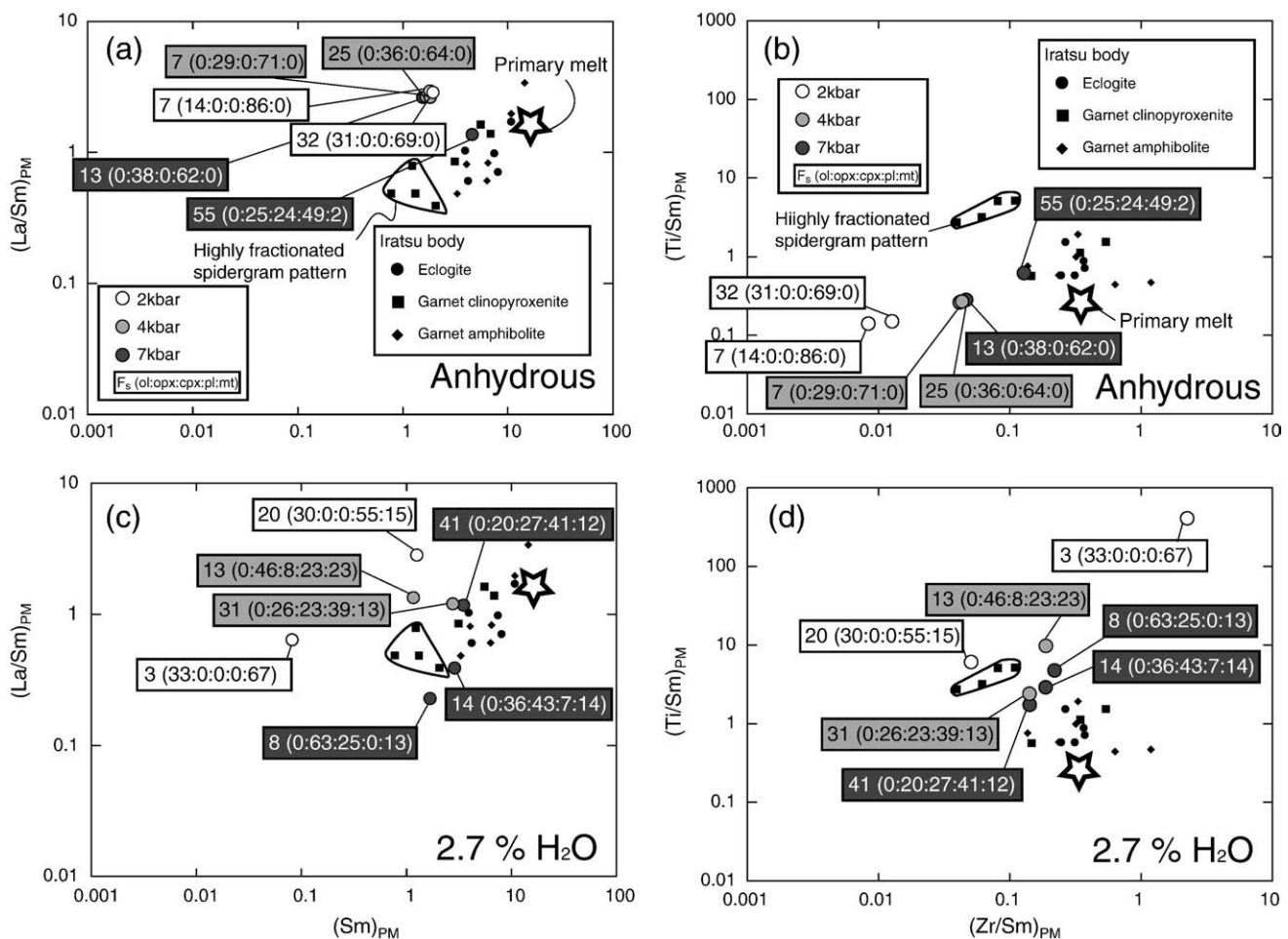


Fig. 11. Possible cumulate compositions estimated by crystallization modeling under various pressures and H₂O contents. Details of modeling are described in the text (Section 6.2.2). The label for individual plot shows solid fraction and mineral mode (wt.% of solid phase). F_s = % solid fraction; ol = olivine; opx = orthopyroxene; cpx = clinopyroxene; pl = plagioclase; mt = magnetite.

clinopyroxene from Hauri et al. (1994). For plagioclase, the average of partition coefficients with high anorthite (An) values ($An\# > 70$) is adopted (Bindeman et al., 1998). Partition coefficient of magnetite is from Nielsen and Beard (2000). Bulk partition coefficients were calculated with these partition coefficients of minerals and mineral mode percentages. It is assumed that the primary trace element abundances are similar to those of eclogite having corresponding $\varepsilon_{Nd}(t)$ value. Sample SD35 ($SiO_2 \sim 49\%$; $\varepsilon_{Nd}(t) = +0.5$) was chosen as the primary melt. We assumed an equilibrium crystallization and calculated cumulate composition with an equation,

$$C_s = C_0 D / (F_s(D-1) + 1)$$

where C_s is the elemental composition in solid (= cumulate), D is the bulk partition coefficient, C_0 is the elemental composition in initial liquid, and F_s is solid fraction. The result is shown in Table 4 and Fig. 11.

Under anhydrous condition and at low pressures, olivine and plagioclase are early crystallization phases. The accumulation of these minerals cannot explain the REE and HFSE characteristics of highly fractionated garnet clinopyroxenites (Fig. 11a and b). Although olivine is replaced by orthopyroxene with increasing pressure, the cumulate composition is also different from the highly fractionated garnet clinopyroxenite. Under a hydrous condition, magnetite is crystallized relatively early. Magnetite crystallization sharply increases $(Ti/Sm)_{PM}$ in cumulate (Fig. 11c and d). At low pressures, the assemblage of olivine + plagioclase + magnetite has $(Ti/Sm)_{PM}$ and $(Zr/Sm)_{PM}$ ratios similar to highly fractionated garnet clinopyroxenites, but, the assemblage has higher $(La/Sm)_{PM}$ ratios (Fig. 11c and d). With increasing pressure, clinopyroxene stability field expands, and clinopyroxene crystallization would decrease $(La/Sm)_{PM}$ in the cumulate. The assemblage of orthopyroxene + clinopyroxene + plagioclase + magnetite has similar trace element ratios to highly fractionated garnet clinopyroxenites (Fig. 11c and d).

Our modeling shows that the accumulation of plagioclase + clinopyroxene + magnetite occurring under the hydrous and high fO_2 condition (~NNO-buffer) in the middle to lower crust could produce a cumulate similar to the protoliths garnet clinopyroxenites from a parental magma of the eclogite composition. Accumulation of magnetite causes Ti enrichment whereas accumulation of plagioclase reduces Zr concentration in the cumulates due to the “dilution effect” of plagioclase which has a very small partition coefficient for Zr (0.002, Table 3). In fact, the presence of positive Eu anomalies in garnet clinopyroxenites is consistent with plagioclase accumulation. The general shape of REE pattern is controlled by clinopyroxene accumulation.

6.2.3. Comparison with modern volcanic sequences

The fact that eclogites and high- SiO_2 garnet amphibolites show HFSE depletion relative to REE suggests that these rocks formed at a subduction-related setting. Since subduction-related magmatism generally occurs under a hydrous and high fO_2 condition, the formation of cumulate could thus be straightforward. The Sr-Nd isotopic compositions of these rocks plot in both oceanic island arc and continental arc basalt fields (Fig. 7). However, eclogites and garnet amphibolites do not have highly negative $\varepsilon_{Nd}(t)$ values, whereas continental arc basalts may have the values extended to -10 by contribution of evolved continental materials.

Fig. 7 shows that eclogites and garnet amphibolites also overlap with the OIB field. The eclogites and garnet amphibolites with lower $\varepsilon_{Nd}(t)$ values do not show significant HFSE depletion (Fig. 10). These features suggest that enriched component of the Iratsu body is similar to enriched mantle rather than evolved continent. The protoliths of the Iratsu body might form in an oceanic island arc setting with a minimum possibility of continental contamination. We concluded that the Iratsu body is not tectonic blocks derived from the hanging wall of pre-Sanbagawa subduction zone, so suggested by Takasu et al.

(1994), but an accretionary part of island arc migrated from the oceanic domain.

The observation that some rocks from the Iratsu body have garnet granulite relics places a strong constraint to the tectonic setting in which the protoliths formed (Yokoyama, 1980; Ota et al., 2004). Because the Sanbagawa metamorphism did not pass through granulite-facies condition, the protoliths had to have undergone a granulite-facies metamorphism before the Sanbagawa metamorphism. This pre-Sanbagawa metamorphism requires a geotherm and litho-pressure of a thick crust (15–30 km, Yokoyama, 1980). The oceanic crust is about 7 km thick generally, but some oceanic island arcs have thick crust of ~30 km (Yamamoto et al., 2009). Eclogites, garnet clinopyroxenites and garnet amphibolites from the Iratsu body are comparable with the accreted and exposed middle-lower crustal rocks of some paleo-island arc sections in the $(Ti/Gd)_{PM}$ – $(Zr/Sm)_{PM}$ plots (Fig. 12). The decoupling between $(Ti/Gd)_{PM}$ and $(Zr/Sm)_{PM}$ of the rocks from the Iratsu body is similar to the middle to lower arc crust.

6.3. Origin and tectonic setting of other rocks

6.3.1. Pelitic schists and gneisses

The pelitic schists are characterized by negative $\varepsilon_{Nd}(t)$ (~−5), LREE enrichment in REE distribution and negative Nb anomalies in spidergram (Figs. 7 and 8). This suggests that the original pelitic sediments were derived from continental materials. The zircon age study of Aoki et al. (2007) indicates that some inherited magmatic zircons from the Sanbagawa psammitic schists yielded dates of 1800–1900 Ma. The geochronological data also support that the source materials of the meta-sediments were derived from an old continental crust. Pelitic gneisses fringing the Iratsu body have geochemical and isotopic characteristics similar to pelitic schist. Therefore, the protoliths of pelitic gneisses are the same as those of the Sanbagawa pelitic schists.

6.3.2. Mafic schists

The protoliths of mafic schists have been regarded as MORB based on the field relation and geochemical characteristics (Okamoto et al., 2000; Nozaki et al., 2006). The geochemical and isotopic data presented in this study divided the mafic schists into two types; the first is comparable to normal (N-) MORB, and the second to enriched (E-) MORB (Figs. 7 and 9). Thus, the protoliths might have formed in a mid-ocean ridge influenced by a plume activity, like the present North Atlantic. Alternatively, back-arc basin is another possible tectonic setting, because the volcanism of back-arc basin generates both

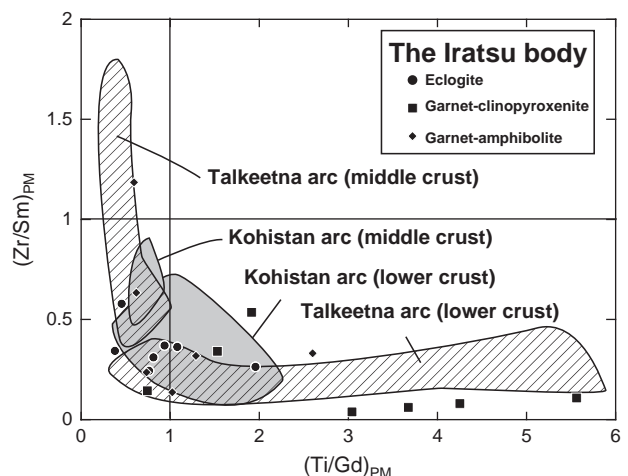


Fig. 12. $(Zr/Sm)_{PM}$ vs. $(Ti/Gd)_{PM}$ diagram showing a comparison between the rocks from the Iratsu body and the lower and middle crust of paleo-oceanic island arc sections. The data of the Talkeetna and Kohistan arcs are from Greene et al. (2006) and Garrido et al. (2006), respectively.

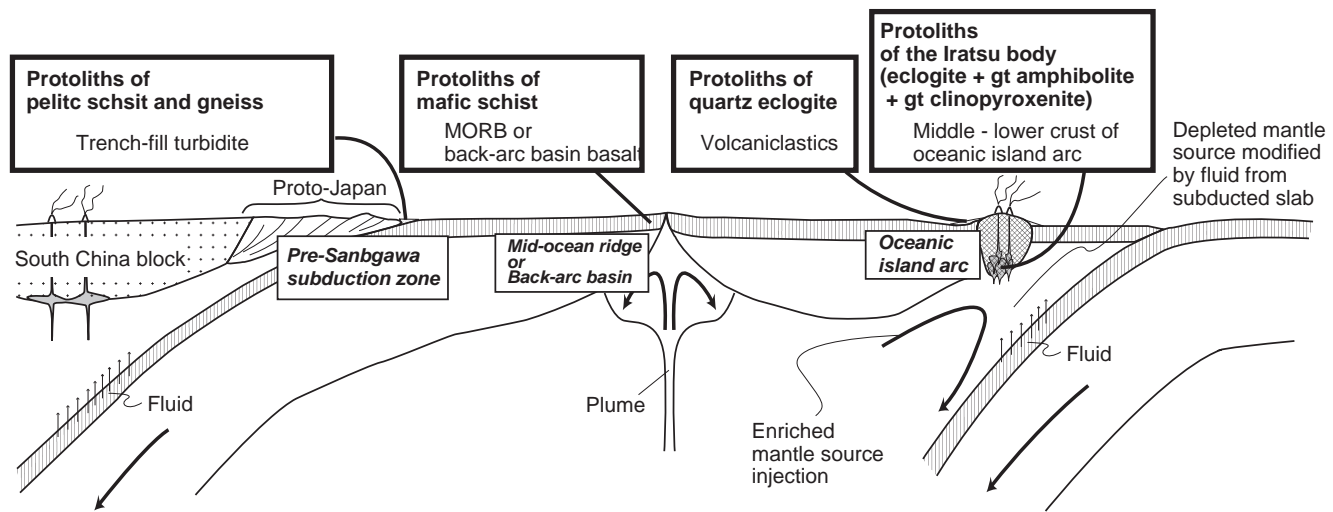


Fig. 13. A tectonic model for the protoliths of eclogites and related rocks from the Besshi area.

MORB- and OIB-type basalts without subduction-related geochemical characteristics (Pearce et al., 1999). Because the mafic schists are overlain by quartz schists whose protoliths are considered to be pelagic cherts (Okamoto et al., 2000), the back-arc should be sufficiently distanced from the continent, so that little amount of terrigenous materials or island arc volcaniclastics could be deposited on the protoliths of the mafic schists.

6.3.3. Quartz eclogites

The origin of quartz eclogites has been discussed. Banno and Yokoyama (1977) suggested that the quartz eclogites formed from a silica-rich residual liquid when the Higashi-Akaishi-Iratu peridotite-gabbro body crystallized from a parental picritic magma. However, because $\epsilon_{\text{Nd}}(t)$ values of quartz eclogites ($\sim +6.5$) are sufficiently different from those of the rocks from the Iratsu body ($\epsilon_{\text{Nd}}(t) = -1$ to $+4$), the quartz eclogites and the Iratsu rocks could not be derived from the same parental magma (Fig. 7). Furthermore, Okamoto et al. (2004) considered that the protoliths of quartz eclogites are trench-filled sediments based on presence of detrital zircons. However, the idea is not supported by the Nd isotopic and trace element geochemical data.

The quartz eclogites are more similar to volcanic rocks of oceanic island arcs. Commonly oceanic island arc basalt has a negative Nb anomaly and juvenile isotopic signature (Pearce et al., 1999). Slightly concave REE patterns of quartz eclogites are similar to those of boninites. Gill et al. (1994) documented that volcaniclastic turbidites from the Izu-Bonin island arc have preserved the geochemical characteristics of igneous sources. Takasu (1989) argued that the protoliths of quartz eclogites are deep-sea pelitic sediments with basaltic volcaniclastics. Thus, the protoliths of quartz eclogites could be volcaniclastic turbidites forming in a setting proximal to oceanic island arc apart from continental margin. Igneous zircons in quartz-rich rocks from the Iratsu body have ages concentrated in the range of 134–148 Ma, except one grain with an Early Proterozoic age (~ 1900 Ma; Okamoto et al., 2004). The peak age (~ 140 Ma) might represent volcanic event.

6.4. Our tectonic model – accretion of deeply subducted oceanic island arc

The possible tectonic settings of the protoliths of rocks from the Besshi area are summarized in Fig. 13. The protoliths of the eclogites, garnet clinopyroxenites and garnet amphibolites from the Iratsu body have two kinds of mantle sources; a depleted component with HFSE depletion and an enriched component without HFSE depletion. The former component is likely a depleted mantle source modified by slab-released fluid; and the latter is an OIB-like asthenospheric mantle

source. Cumulate rocks were the result of crystal accumulation under high fO_2 and H_2O contents in the middle to lower crust. Consequently, the most plausible tectonic setting of the Iratsu body is an oceanic island arc. Hattori et al. (2010) carried out a chemical study on the whole-rocks and minerals of ultramafic rocks from the Higashi-Akaishi body. They suggested that the ultramafic rocks represented refractory peridotite formed as the result of high degree of partial melting and part of a root of an arc. Although the origin of ultramafic rocks was regarded as a hanging-wall mantle (Hattori et al. 2010), it is also likely that the ultramafic rocks are residue of the protoliths of the Iratsu body.

Quartz eclogites are considered to be volcanic turbidites deposited at a foot of the oceanic island arc. The protoliths of mafic schists might form in a mid-ocean ridge influenced by a plume, or in a back-arc basin. The protoliths of pelitic schists and pelitic gneisses were likely deposited proximal to a continental arc and should be trench-fill turbidite.

When an island arc is introduced to a subduction zone, it had been considered that an island arc could not be subducted due to high buoyancy and collided with the counter continent or arc. Yamamoto et al. (2009) presented the idea that which collision or subduction of an island arc depend on the dynamic conditions. In the case that an arc is parallel to a subduction zone, the arc would collide with continental margin (e.g., Celebes), however, in the case of oblique or orthogonal subduction of an island arc less than 30 km thick, the island arc would be subducted into mantle (e.g., Kyushu-Palau). The Iratsu body should represent a deeply subducted and accreted island arc in the eclogite-facies P-T condition. During the subduction, the trench-fill turbidites and volcaniclastics were involved into the margin of the Iratsu body and metamorphosed to pelitic gneisses and quartz eclogites, respectively.

Acknowledgement

We greatly appreciate S. Maruyama for giving us the opportunity to use his sample collection. We are deeply grateful to S.-L. Chung and C.-Y. Lee for making available their laboratory facilities for chemical analyses presented in this study. Laboratory assistances of W.-Y. Hsu, I.-J. Lin and F.-L. Lin are highly acknowledged. Reviews from Dr. S.R. Wallis and an anonymous reviewer and comments by R. Rudnick greatly improved this manuscript. This work was supported by the National Science Council (Taiwan) research grants to Bor-ming Jahn (NSC98-2116-M-001-009 and NSC97-2116-M-001-003).

Appendix A. XRF analysis

Lee et al. (1997) carried out the duplicate analyses on the USGS standards RGM-1 and W-2. The result is shown in Table A1. Relative

Table A1

Duplicated analyses on USGS standard samples by Lee et al. (1997).

	1	2	3	4	5	6	7	8	9	10	Ave.	SD (1σ)	RSD (%)	Recommended value ^a
<i>RGM-1</i>														
SiO ₂	73.29	73.42	73.49	73.35	73.29	73.29	73.42	73.49	73.35	73.29	73.37	0.081	0.11	73.50
TiO ₂	0.28	0.28	0.28	0.28	0.27	0.28	0.28	0.27	0.28	0.28	0.003	0.94	0.27	
Al ₂ O ₃	14.22	14.22	14.21	14.21	14.19	14.22	14.22	14.21	14.21	14.19	14.21	0.010	0.07	13.80
Fe ₂ O ₃ *	1.73	1.72	1.73	1.72	1.72	1.73	1.73	1.72	1.72	1.72	1.72	0.002	0.13	1.89
MnO	0.04	0.04	0.04	0.04	0.04	0.04	0.04	0.04	0.04	0.04	0.04	0.000	1.18	0.04
MgO	0.23	0.22	0.23	0.24	0.24	0.22	0.23	0.23	0.24	0.24	0.23	0.006	2.63	0.28
CaO	1.22	1.22	1.21	1.22	1.21	1.22	1.22	1.21	1.21	1.22	1.21	0.004	0.34	1.15
Na ₂ O	4.01	3.94	4.06	4.00	3.99	4.06	3.94	4.01	3.99	4.00	4.00	0.041	1.04	4.12
K ₂ O	4.22	4.22	4.21	4.21	4.22	4.22	4.21	4.21	4.21	4.21	4.21	0.004	0.10	4.35
P ₂ O ₅	0.06	0.06	0.06	0.06	0.06	0.06	0.06	0.06	0.06	0.06	0.06	0.001	1.26	0.05
<i>W-2</i>														
SiO ₂	52.08	52.10	52.01	52.08	52.11	52.01	52.10	52.08	52.08	52.11	52.08	0.036	0.07	52.70
TiO ₂	1.09	1.09	1.08	1.08	1.09	1.09	1.09	1.08	1.08	1.09	1.08	0.005	0.47	1.06
Al ₂ O ₃	15.44	15.42	15.45	15.45	15.47	15.45	15.42	15.44	15.45	15.47	15.45	0.016	0.10	15.45
Fe ₂ O ₃ *	10.83	10.84	10.83	10.83	10.84	10.83	10.84	10.83	10.83	10.84	10.83	0.005	0.04	10.80
MnO	0.16	0.17	0.16	0.16	0.16	0.16	0.17	0.16	0.16	0.16	0.16	0.001	0.77	0.17
MgO	6.38	6.43	6.45	6.40	6.38	6.38	6.43	6.45	6.40	6.38	6.41	0.029	0.45	6.37
CaO	11.01	11.00	11.02	11.01	11.01	11.01	11.00	11.02	11.01	11.01	11.01	0.005	0.05	10.86
Na ₂ O	2.16	2.19	2.18	2.20	2.18	2.16	2.20	2.18	2.19	2.18	2.18	0.014	0.65	2.20
K ₂ O	0.60	0.61	0.60	0.60	0.60	0.60	0.60	0.61	0.60	0.60	0.60	0.001	0.25	0.63
P ₂ O ₅	0.14	0.14	0.14	0.14	0.14	0.14	0.14	0.14	0.14	0.14	0.14	0.002	1.35	0.14

^a Govindaraju, K., 1994. Compilation of working values and sample description for 383 geostandards. *Geostandards Newsletter*, 18, 1–158.

standard deviation (RSD) was below 3% (1σ) for all elements and reproduced the recommended values within 5% for most elements.

References

- Aoki, K., Iizuka, T., Hirata, T., Maruyama, S., Terabayashi, M., 2007. Tectonic boundary between the Sanbagawa belt and the Shimanto belt in central Shikoku, Japan. *Journal of the Geological Society of Japan* 113, 171–183.
- Aoya, M., Tsuboi, M., Wallis, S.R., 2006. Origin of eclogitic metagabbro mass in the Sanbagawa belt: geological and geochemical constraints. *Lithos* 89, 107–134.
- Aoya, M., Uehara, S., Matsumoto, M., Wallis, S.R., Enami, M., 2003. Subduction-stage pressure-temperature path of eclogite from the Sanbagawa belt: prophetic record for oceanic-ridge subduction. *Geology* 31, 1045–1048.
- Banno, S., Sakai, C., 1989. Geology and metamorphic evolution of the Sanbagawa metamorphic belt, Japan. In: Daly, J.S., Cliff, R.A., Yardley, B.W.D. (Eds.), *Evolution of Metamorphic Belts*. Special Publications, vol. 43. Geological Society, London, pp. 519–532.
- Banno, S., Yokoyama, K., 1977. Peridotite-metamorphic evolution of the Sanbagawa metamorphic belt, Japan. In: Hide, K. (Ed.), *The Sanbagawa belt*. Hiroshima University Press, Hiroshima, pp. 57–68.
- Bindeman, I., Davis, A.M., Drake, M.J., 1998. Ion microprobe study of plagioclase–basalt partition experiments at natural concentration levels of trace elements. *Geochimica et Cosmochimica Acta* 62, 1175–1193.
- Dallmeyer, R.D., Takasu, A., 1991. Tectonometamorphic evolution of the Sebadani eclogitic metagabbro and the Sanbagawa schists, central Shikoku Japan; $^{40}\text{Ar}/^{39}\text{Ar}$ mineral age constraints. *Journal of Metamorphic Geology* 9, 605–618.
- Enami, M., Wallis, S.R., Banno, Y., 1994. Paragenesis of sodic pyroxene-bearing quartz schists: implications for the P-T history of the Sanbagawa belt. *Contributions to Mineralogy and Petrology* 116, 182–198.
- Endo, S., Wallis, S.R., Hirata, T., Anczkiewicz, R., Platt, J., Thirlwall, M., Asahara, Y., 2009. Age and early metamorphic history of the Sanbagawa belt: Lu–Hf and P–T constraints from the Western Iwatsuki eclogite. *Journal of Metamorphic Geology* 27, 371–384.
- Frei, D., Liebscher, A., Franz, G., Wunder, B., Klemme, S., Blundy, J., 2009. Trace element partitioning between orthopyroxene and anhydrous silicate melt on the lherzolite solidus from 1.1 to 3.2 GPa and 1230 to 1535 °C in the model system Na₂O–CaO–MgO–Al₂O₃–SiO₂. *Contributions to Mineralogy and Petrology* 157, 473–490.
- Garrido, C.J., Bodinier, J.-L., Burg, J.-P., Zeilinger, G., Hussain, S.S., Dawood, H., Chaudhry, M.N., Gervilla, F., 2006. Petrogenesis of mafic garnet granulite in the lower crust of the Kohistan paleo-arc complex (northern Pakistan): implications for intra-crustal differentiation of island arcs and generation of continental crust. *Journal of Petrology* 47, 1873–1914.
- Gill, J.B., Hiscock, R.N., Vidal, Ph., 1994. Turbidite geochemistry and evolution of the Izu–Bonin arc and continents. *Lithos* 33, 135–168.
- Green, T.H., Adam, J., 2003. Experimentally-determined trace element characteristics of aqueous fluid from dehydration mafic oceanic crust at 3.0 GPa, 650–700 °C. *European Journal of Mineralogy* 15, 815–830.
- Greene, A.R., DeBari, S.M., Kelemen, P.B., Blusztajn, J., Clift, P.D., 2006. A detailed geochemical study of island arc crust: the Talkeetna arc section, south-central Alaska. *Journal of Petrology* 47, 1051–1093.
- Hamada, M., Fujii, T., 2008. Experimental constraints on the effects of pressure and H₂O on the fractional crystallization of high-Mg island arc basalt. *Contributions to Mineralogy and Petrology* 155, 767–790.
- Hattori, K., Wallis, S.R., Enami, M., Mizukami, T., 2010. Subduction of mantle wedge peridotites: evidence from the Higashi-Akaishi ultramafic body in the Sanbagawa metamorphic belt. *The Island Arc* 19, 192–207.
- Hauri, E.H., Wagner, T.P., Grove, T.L., 1994. Experimental and natural partitioning of Th, U, Pb and other trace elements between garnet, clinopyroxene and basaltic melts. *Chemical Geology* 117, 149–166.
- Hermann, J., Spandler, C., Hack, A., Korsakov, A.V., 2006. Aqueous fluids and hydrous melts in high-pressure and ultra-high pressure rocks: implications for element transfer in subduction zones. *Lithos* 92, 399–417.
- Higashino, T., 1990. The higher grade metamorphic zonation of the Sanbagawa metamorphic belt in central Shikoku, Japan. *Journal of Metamorphic Geology* 8, 413–423.
- Isozaki, Y., 1996. Anatomy and genesis of a subduction-related orogen: a new view of geotectonic subdivision and evolution of the Japanese islands. *The Island Arc* 5, 289–320.
- Isozaki, Y., Maruyama, M., 1991. Studies on orogeny based on plate tectonics in Japan and new geotectonic subdivision of the Japanese islands. *Journal of Geography* 100, 697–761 (in Japanese with English abstract).
- Itaya, T., Takasugi, H., 1988. Muscovite K–Ar ages of the Sanbagawa schists, Japan and argon depletion during cooling and deformation. *Contributions to Mineralogy and Petrology* 100, 281–290.
- Jahn, B.-m., Bernard-Griffiths, J., Charlot, R., Cornichet, J., Vidal, F., 1980. Nd and Sr isotopic compositions and REE abundances of Cretaceous MORB (Holes 417D and 418A, Leg 51 and 53). *Earth and Planetary Science Letters* 48, 171–184.
- Kawato, K., Isozaki, Y., Itaya, T., 1991. Geotectonic boundary between the Sanbagawa and Chichibu belts in central Shikoku, Southwest Japan. *Journal of the Geological Society of Japan* 97, 959–975 (in Japanese with English abstract).
- Kelemen, P.B., Hanghøj, K., Greene, A.R., 2003. One view of the geochemistry of subduction-related magmatic arcs, with an emphasis on primitive andesite and lower crust, in: Rudnick, R.L. (Ed.), *The Crust*, in: Holland, H.D., Turekian, K.K. (Eds.), *Treatise on Geochemistry*, Elsevier-Pergamon, Oxford, vol. 3, pp. 1–70.
- Kiminami, K., Ishihama, S., 2003. The parentage of low-grade metasediments in the Sanbagawa metamorphic belt, Shikoku, southwest Japan, based on whole-rock geochemistry. *Sedimentary Geology* 159, 257–274.
- Kogiso, T., 2007. A geochemical and petrological view of mantle plume. In: Yuen, D.A., Maruyama, S., Karato, S., Windley, B.F. (Eds.), *Superplume: Beyond Plate tectonics*. Springer, Dordrecht, pp. 165–186.
- Lee, C.Y., Tsai, J.H., Ho, H.H., Yang, T.F., Chung, S.L., 1997. Quantitative analysis in rock samples by X-ray fluorescence spectrometer (I) major elements. Program with Abstracts of 1997 Annual Meeting of Geological Society of China, Taipei, pp. 418–420 (in Chinese).
- Minamishin, M., 1979. Whole-rock Rb–Sr ages of the Sanbagawa schists in the Asemi area central Shikoku (Abstract). *Journal of Association of Mineralogy, Petrology, and Economic Geology*, 74, p. 153 (in Japanese).
- Nielsen, R.L., Beard, J.S., 2000. Magnetite–melt HFSE partitioning. *Chemical Geology* 164, 21–34.
- Nozaki, T., Nakamura, K., Awaji, S., Kato, Y., 2006. Whole-rock geochemistry of basic schists from the Beishi area, central Shikoku: implications for the tectonic setting of the Beishi sulfide deposit. *Resource Geology* 56, 423–432.
- Okamoto, K., Maruyama, S., Isozaki, Y., 2000. Accretionary complex origin of the Sanbagawa, high P/T metamorphic rocks, central Shikoku, Japan – layer-parallel shortening structure and greenstone geochemistry. *Journal of the Geological Society of Japan* 106, 70–86.

- Okamoto, K., Shinjoe, H., Katayama, I., Terada, K., Sano, Y., 2004. SHRIMP U–Pb dating of quartz-bearing eclogite from the Sanbagawa belt, south-west Japan: implications for metamorphic evolution of subducted protolith. *Terra Nova* 16, 81–89.
- Ota, T., Terabayashi, M., Katayama, I., 2004. Thermobaric structure and metamorphic evolution of the Iraatsu eclogite body in the Sanbagawa belt, Central Shikoku, Japan. *Lithos* 73, 95–126.
- Pearce, J.A., Kempton, P.D., Nowell, G.M., Noble, S.R., 1999. Hf–Nd element and isotope perspective on the nature and provenance of mantle and subduction components in Western Pacific arc-basin system. *Journal of Petrology* 40, 1579–1611.
- Sasaki, H., Isozaki, Y., 1992. Low-angle thrust between the Sanbagawa and Shimanto belts in central Kii peninsula, southwest Japan. *Journal of the Geological Society of Japan* 98, 57–60 (in Japanese).
- Senda, R., Kachi, T., Tanaka, T., 2006. Multiple records from osmium, neodymium, and strontium isotope systems of the Nikubuchi ultramafic complex in the Sambagawa metamorphic belt, central Shikoku, Japan. *Geochemical Journal* 40, 135–148.
- Spandler, C., Hermann, J., Arculus, R., Mavrogenis, J., 2003. Redistribution of trace elements during prograde metamorphism from lawsonite blueschist to eclogite facies: implications for deep subduction zone processes. *Contributions to Mineralogy and Petrology* 146, 205–222.
- Sun, S.-S., McDonough, W.F., 1989. Chemical and isotopic systematics of oceanic basalts; implications for mantle composition and processes. In: Saunders, A.D., Norry, M.J. (Eds.), *Magmatism in the ocean basins*. : Special Publications, vol. 42. Geological Society, London, pp. 313–345.
- Takasu, A., 1989. P–T histories of peridotite and amphibolite tectonic blocks in the Sambagawa metamorphic belt, Japan. In: Daly, J.S., Cliff, R.A., Yardley, B.W.D. (Eds.), *Evolution of Metamorphic Belts*. : Special Publications, vol. 43. Geological Society, London, pp. 533–538.
- Takasu, A., Dallmeyer, R.D., 1990. ^{40}Ar – ^{39}Ar age constraints for the tectono-thermal evolution of the Sambagawa metamorphic belt, central Shikoku, Japan: a Cretaceous accretionary prism. *Tectonophysics* 185, 303–324.
- Takasu, A., Wallis, S.R., Banno, S., Dallmeyer, R.D., 1994. Evolution of the Sambagawa metamorphic belt, Japan. *Lithos* 33, 119–133.
- Terabayashi, M., Okamoto, K., Yamamoto, H., Kaneko, Y., Ota, T., Maruyama, S., Katayama, I., Komiya, T., Ishikawa, A., Anma, R., Ozawa, H., Windley, B.F., Liou, J.G., 2005. Accretionary complex origin of the mafic–ultramafic bodies of the Sanbagawa belt, Central Shikoku, Japan. *International Geology Review* 47, 1058–1078.
- Wallis, S.R., Aoya, M., 2000. A re-evaluation of the eclogite facies metamorphism in SW Japan: proposal for an eclogite nappe. *Journal of Metamorphic Geology* 18, 653–664.
- Wallis, S.R., Anczkiewicz, R., Endo, S., Aoya, M., Platt, J.P., Thirlwall, M., 2009. Plate movements, ductile deformation and geochronology of the Sanbagawa belt, SW Japan: tectonic significance of 89–88 Ma Lu–Hf eclogite ages. *Journal of Metamorphic Geology* 27, 93–105.
- Wallis, S.R., Moriyama, Y., Tagami, T., 2004. Exhumation rates and age of metamorphism in the Sanbagawa belt: new constraints from zircon fission track analysis. *Journal of Metamorphic Geology* 22, 17–24.
- Yamamoto, H., Okamoto, K., Kaneko, Y., Terabayashi, M., 2004. Southward extrusion of eclogite-bearing mafic–ultramafic bodies in the Sanbagawa belt, central Shikoku, Japan. *Tectonophysics* 387, 151–168.
- Yamamoto, S., Senshu, H., Rino, S., Omori, S., Maruyama, S., 2009. Granite subduction: arc subduction, tectonic erosion and sediment subduction. *Gondwana Research* 15, 443–453.
- Yang, J.H., Chung, S.L., Wilde, S.A., Wu, F.Y., Chu, M.F., Lo, C.H., Fan, H.R., 2005. Petrogenesis of post-orogenic syenites in the Sulu Orogenic Belt, east China: geochronological, geochemical and Nd–Sr isotopic evidence. *Chemical Geology* 214, 99–125.
- Yokoyama, K., 1980. Nikubuchi peridotite body in the Sanbagawa metamorphic belt; thermal history of the ‘Al–pyroxene-rich suite’ peridotite body in high pressure metamorphic terrain. *Contributions to Mineralogy and Petrology* 73, 1–13.
- Zanetti, A., Tiepolo, M., Oberti, R., Vannucci, R., 2004. Trace-element partitioning in olivine: modeling of a complete data set from a synthetic hydrous basanite melt. *Lithos* 75, 39–54.